Fast Inactivation by Light-Inducible Protein Auto-ubiquitination

Ana Filipa Martins dos Santos

September, 2019

Integrated Masters in Bioengineering
• Molecular Biotechnology •

U.PORTO
INSTITUTO DE CIÊNCIAS BIOMÉDICAS ABEL SALAZAR UNIVERSIDADE DO PORTO
FEUP FACULDADE DE ENGENHARIA UNIVERSIDADE DO PORTO
INSTITUTO DE INVESTIGAÇÃO E INOVAÇÃO EM SAÚDE UNIVERSIDADE DO PORTO

Ana Filipa Martins dos Santos

Fast Inactivation by Light-Inducible Protein Auto-ubiquitination

Integrated Masters in Bioengineering
• Molecular Biotechnology •

Faculty of Engineering
Institute for the Biomedical Sciences Abel Salazar
University of Porto

Supervision

Eurico Morais-de-Sá, PhD

Principal Researcher & Group Leader
Epithelial Polarity & Cell Division
i3S - Instituto de Investigação e Inovação em Saúde

Co-supervision

Mariana Osswald, MSc

PhD Student
Epithelial Polarity & Cell Division
i3S - Instituto de Investigação e Inovação em Saúde

September, 2019

▪ Blank page ▪

Escravos cardíacos das estrelas,
Conquistamos todo o mundo antes de nos levantar da cama;
Mas acordamos e ele é opaco

Álvaro de Campos, *in* Tabacaria

When one has weighed the sun in the balance, and measured the steps of the moon, and mapped out the seven heavens star by star, there still remains oneself. Who can calculate the orbit of his own soul?

Oscar Wilde, *in De profundis*

▪ Blank page ▪

Aknowledgments

John Donne famously wrote that "No man is an island entire of itself". Over the course of my short life, I have been a part of teams of many kinds, towards many different purposes. Never would I have guessed that Donne's words would become the most evident to me when writing a supposedly individual document. This thesis will be submitted with one author on the cover. Make no mistake: that is absolutely untrue. None of it could have been possible had I stood alone.

My first thank you obviously goes to Eurico and Mariana for being, in every way possible, the best supervisors anyone could ask for. You are the reason this thesis could only have been written in the plural form. I am so unworthy of the great patience, time, dedication, and helpfulness you have shown from the very beginning. You make a great team, and between the both of you, you have provided a strong, reliable safety net for all my crises (even the non-work related ones). I left every single meeting (and there sure were many) feeling reassured, and less lost. And most of all, I was lucky to have been blessed with two supervisors who were not only available, but also competent and capable of pertinent critical judgement at all times (and the two things do not always go hand-in-hand). "Thank you" is not enough (maybe I can bake in the future to help make it up to you?).

To every single member of the EPCD & CDGS family: I look up to each of you and it was an honour and a privilege, to work side by side with you. Thank you, in no particular order: to the very politically incorrect Carlos, for having brought me here in the first place (and for tolerating my annoying existence in general, and for being funnier than I would like to admit); to the almighty professor Claudio Sunkel, whose amazing classes were the start of this all; to Augusta for always being there to kindly attend to every need and making everything run smoothly; to Sofia Silva for keeping me company during my late hours in the lab, even without knowing (that spontaneous singing and kind quirkiness!); to Moops, my OCD partner, for her help and keen insight on the inner workings of the lab; to Sofia Moreira for sharing her poetry, her heart and her warmth with me so many times; to Tália, who won my heart over in such a small amount of time (it takes a crazy person to know a crazy person); to my "guetto" partners Nélson, Ana, Ana Maria, and Vítor for all the non-working, the inside jokes, the tips, the help, the soundtracks, and, above all, the crazy conversations that went on outside the lab; to Margarida G., Rita, Mafalda, Pedro, João, to all of you in general for making this the "Happy Lab" indeed, for all the laughter, the kindness, the concern, for your thoughtful insights during lab meetings, and for your professionalism and competence. Finally, I leave a very warm thank you to my "little lab brother" (who was, from the start, much better than I will ever be) for his presence, help and support, and for being an example of resilience and enthusiasm. I am so proud of you.

Nem só de trabalho se faz uma tese, e se o laboratório funcionou tantas vezes como uma segunda casa, foram todas as pessoas que se seguem que sustentaram e sustentam, nos bastidores, as partes de mim de que menos me orgulho, para que pudesse, cá fora, ir funcionando qualquer coisita, ao bater da claquete. Esta tese (e tudo o resto) não teria, certamente, sido possível sem vós.

Obrigada aos meus pais, por (ainda) não me terem posto fora de casa, por aguentarem e perdoarem todas as ausências, o ter chegado fora de horas, o ter ficado horas a mais, o sono por excesso e por defeito, o cansaço, a falta de tempo e muitas vezes de paciência e por terem segurado a casa quando eu não soube, não pude ou não consegui, ajudar sequer um pouco. Obrigado também aos meus irmãos, à minha cunhada e à Isabel, minha segunda mãe, pelo orgulho e pela preocupação que demonstram, consistentemente, cada um à sua maneira e por gostarem tanto de mim, mesmo quando não mereço.

Márcia, obrigada por teres desbravado comigo o mato acrílico desta cidade e de outras, em busca da Arte e de todas as coisas estranhas que vimos e eu nem sei classificar, por ter sido da tua natureza ser vista comigo pelos porteiros do i3s às horas mais inauditas, por viveres no Paraíso e o partilhares comigo, pela tua ajuda em todos os trabalhos e exames, e nesta tese (se não fossem os tomates-cereja...), pelo Chandler que vive na tua cabeça, pelo macaquinho da procrastinação que me emprestas tantas vezes (é uma honra procrastinar contigo!), pelos atrasos, pela comida, pelas boleias, pelo teu sofá para dormir… Em suma, porque és e foste, de todas as vezes, exactamente aquilo de que eu precisava e não sabia.

Obrigada aos companheiros de curso que se tornaram muito mais do que isso: ao Abel (se eu não entregasse esta tese, tu nunca me perdoarias) e à Marta (a minha mãe desnaturada favorita), por terem tornado este curso suportável e porque já me esqueci de tudo o que aprendi nas aulas, mas nunca me vou esquecer de vocês. E ainda à Joana, que me acompanhou nesta recta final numa porção de desabafos aleatórios.

Um agradecimento especial aos meus amigos pela paciência, pelas conversas, lágrimas e risos e por terem atendido o telefone, aberto a casa e o coração às horas e pedidos mais inóspitos: ao meu "BFF" (que moldou tanto do que fui e do que sou e me fez tanta companhia no recantos da insanidade); ao JP e à Isa, que já são prata da casa no meu coração; à minha linda, excêntrica, improvável Dory e ao meu querido e fiel Pedro, por terem estado tão presentes através dos km e me terem apoiado até no embalo da saudade.

E como qualquer poeta que se preze, agradeço finalmente às minhas duas mais recentes musas. Grazie mille, caro mio, por teres entrado na minha vida do avesso, como tudo o que vestes, e teres ficado sem pedir licença, por teres sido ninho (com direito a café) para eu pousar a cabeça e a mochila, por teres entendido tanto, e teres perdoado tanto do que não entendias, por teres sido apeadeiro nas pausas do meu nomadismo. E obrigada a ti, meu Rei do Olimpo, por teres calibrado sem retorno a bússola da minha alma pelo magnetismo da loucura, por me teres mostrado, sem paternalismo ou condescendência, como fazer da vida uma obra de Arte - *And everything I ever did was just another way to scream your name*.

▪ Blank page ▪

▪ Blank page ▪

Abstract

The use of technologies that can effectively interfere with protein activity constitutes a powerful tool in probing protein function. However, current systems employed in conditional protein inactivation do not present kinetics compatible with the study of highly dynamic processes, such as cell division. The aim of this thesis was to develop and validate a novel tool that could be employed in rapid endogenous protein degradation, in a spatio-temporal controlled fashion, by optogenetic targeting of proteins of interest to the cellular degradation machinery. To this purpose, we conceived a system based on the photoswitcheable cryptochrome-2 (CRY2), which is activated and homo-dimerised when exposed to blue-light. CRY2 was fused to Tri-Partite Motif Containing protein 21 (TRIM21), a protein with E3 ligase activity, whose auto-ubiquitination subsequent degradation is associated with oligomerisation. We evaluated the kinetics of different optogenetic modules in their conditional response to a light stimulus and ability to elicit aggregate-induced degradation through live imaging of S2 *Drosophila* cells. We have shown that C-terminal fusion of TRIM21 directly to CRY2, optimised with a small clustering enhancing peptide (Clust) is the most effective way of achieving proteasome-mediated degradation with high temporal resolution. Additionally, we explored TRIM21 subdomains for their potential as minimal functional subunits, and analysed the effects of TRIM21 auto-ubiquitination in overall system efficiency. We then fused an anti-green fluorescent protein (GFP) nanobody, V_HH, to our module, to allow versatile targeting and recruitment of GFP-tagged proteins of interest to the light-induced clusters. The resulting V_HH-CRY2Clust-TRIM module was effective at depleting GFP-tagged atypical Protein Kinase C (aPKC) upon light-activation, reducing the pool of initial protein by 70% within 1 hour. Finally, we applied the system to interfere with intercellular adhesion molecule Echinoid (Ed), having achieved light-triggered reduction of Ed-mediated adhesions in S2 *Drosophila* cells. Additionally, we have also shown that a CRY2-based light triggered clustering system can be employed in co-clustering assays to probe protein-protein interactions. In sum, the developed system proved to be a versatile tool with unprecedented potential for acute disruption of protein function involved in highly dynamic processes.

▪ Blank page ▪

Resumo

A aplicação de tecnologias capazes de interferir eficazmente com a actividade de proteínas constitui uma ferramenta poderosa no esclarecimento da sua função. No entanto, os sistemas actualmente disponíveis para inactivação condicional de proteínas não possuem um perfil cinético compatível com o estudo de processos altamente dinâmicos, tais como a divisão celular. O objectivo desta tese foi o desenvolvimento e validação de uma nova ferramenta aplicável à degradação rápida de proteínas endógenas, com alto controlo espacio-temporal, através do recrutamento optogenético de proteínas de interesse para a maquinaria celular de degradação. Para este efeito, foi concebido um sistema baseado na molécula foto-sensível cryptochrome-2 (CRY2), que é activada e homodimerisada quando exposta a luz azul. O CRY2 foi fundido com a proteína Tri-Partite Motif Containing-21 (TRIM21), com actividade de E3 ligase, cuja auto-ubiquitinação e consequente degradação está relacionada com a sua oligomerisação. A cinética de agregação foto-mediada e a capacidade de induzir a degradação de agregados foram testadas para vários módulos optogenéticos através de microscopia *live* de células S2 de *Drosophila*. Foi demonstrado que a fusão C-terminal do TRIM21 directamente com o CRY2, optimizado por um pequeno péptido que reforça a agregação (Clust), é a forma mais eficaz de induzir degradação mediada pelo proteossoma, com alta resolução temporal. Adicionalmente, os sub-domínios do TRIM21 foram testados pelo seu potencial enquanto unidades funcionais mínimas, e os efeitos da auto-ubiquitinação do TRIM21 sobre a eficiência do sistema foram avaliados. Foi depois fundido ao sistema um anticorpo anti-green fluorescent protein (GFP), V_HH, de modo a permitir o reconhecimento e recrutamento de proteínas de interesse marcadas com GFP para os agregados induzidos por luz. O módulo V_HH-CRY2Clust-TRIM resultante foi capaz de depletar os níveis iniciais de atypical Protein Kinase C (aPKC) fundida com GFP em 70%, no espaço de uma hora. Finalmente, o sistema foi aplicado à molécula de adesão intercelular Echinoid (Ed), tendo-se obtido uma redução de células S2 aderidas por acção do Ed, através da aplicação da luz. Foi ainda demonstrada a utilização de um sistema baseado no CRY2 em ensaios de co-agregação para a detecção de interacções proteicas. Em suma, o sistema desenvolvido demonstrou ser uma ferramenta versátil, com potencial único na interferência aguda sobre a função de proteínas envolvidas em processos de alto dinamismo temporal.

▪ Blank page ▪

Table of contents

List of figures

List of tables

Abbreviation list

aPKC	Atypical protein kinase C
CaMKIIα	Calmodulin-dependent protein kinase IIα
CIBN	Cryptochrome-interacting bHLH N-terminal
CRY2	Cryptochrome-2
Ed	Echinoid
LARIAT	Light-activated reversible inhibition by assembled trap
MP	Multimeric protein
Par6	Partitioning defective protein 6
POI	Protein of interest
RING	Really interesting new gene
TRIM21	Tripartite motif family protein 21, or Ro52 protein
Ub	Ubiquitin
UPS	Ubiquitin-proteasome system
VHH or V_HH	Anti-GFP single domain nanobody

▪ Blank page ▪

CHAPTER I

Introduction and general aims

▪ Blank page ▪

Mechanistic understanding of most biological processes heavily relies on the identification of the molecular players at stake, as well as on the thorough dissection of their expression, function and interaction dynamics over time and space. To this purpose, the application of technologies that can effectively interfere with protein activity constitutes an essential, powerful tool in probing protein function and thereby understanding biological mechanisms at the molecular level.

For years now, the classical approach to protein perturbation has been the employment of genetic engineering, operating at the level of the gene or transcribed product to overexpress, knockdown, or altogether knock-out proteins of interest (POI) (**Campbell et al.**, 2016; **Clift et al.**, 2017). Function identification follows by looking at the consequences of these perturbations as alterations in phenotype, signalling or gene expression patterns (**Röth et al.**, 2019).

However, the use of genomic or transcriptional modulation to interfere with protein function has several disadvantages and limitations in applicability. To tackle these problems, alternative approaches that rely on targeting protein post-translationally have been developed, and constitute an expanding and promising field (**Röth et al.**, 2019).

The purpose of this work was to develop and validate a novel tool that could be employed in rapid endogenous protein degradation *in vivo*, in a spatio-temporal controlled fashion, by recruitment of cellular degradation machinery combined with optogenetics.

Importantly, this work was developed for ultimate application in research on dynamic cellular events, such as cell division or polarisation. These dynamic contexts would require high temporal resolution of protein inactivation, and often require dissection of the function of membrane-bound proteins involved in strong physical interactions. These needs drove the optimisation of a robust tool that can hopefully be of use in a very broad spectrum of research fields and contexts.

Pre-translational modulation: a toolkit with room for improvement

Historically, the ability to interfere with protein function was built upon the central dogma of molecular biology, which highlights the three levels of informational flow in a simple, yet powerful "DNA makes RNA and RNA makes protein" structure. Classically, protein function probing has therefore relied on genome-editing technologies, which act upstream in this process, at the DNA level. Technologies such as zinc-finger nucleases, transcription activator-like effector nucleases, and, more recently, the **C**lustered **R**egularly **I**nterface **P**alindromic **R**epeats (CRISPR)-associated protein Cas9 system have enabled refined DNA manipulation. These systems essentially rely on the ability to introduce double-strand breaks, which then drive cellular DNA repair pathways, allowing for gene knockdown, for example, by base insertions or deletions (**Gaj et al.**, 2016). Alternatively, researchers have long been using transcriptomic approaches such as **RNA i**nterference (RNAi) to achieve gene silencing. RNAi is an endogenous cellular process that essentially uses double-stranded RNA to guide the degradation of mRNA transcripts of POIs (**Heigwer et al.**, 2018).

Even though well-established genetic and transcriptomic approaches have unquestionably played a key role in research, and were behind important breakthroughs and developments in a broad spectrum of fields, they present several the disadvantages and limitations, which have been extensively reviewed, from multiple points of view (**Banaszynski et al.**, 2006; **Campbell et al.**, 2016; **Natsume et al.**, 2016; **Rakhit et al.**, 2014; **Röth et al.**, 2019; **Toure et al.**, 2016). These reviews have outlined that genetic approaches to protein disruption, despite being generally robust and specific, present limitations when applied to core-essential genes, whose knock-down often results in lethality. Furthermore, the slow establishment of genetic knock-downs opens way to genetic compensatory responses and results in irreversible disruption. This can complicate the interpretation of phenotypes, since changes can be attributable to either the loss of the POI or to pleiotropic adaptation that occurred in response to the slow knock-down process.

Transcriptional approaches such as RNAi, can be implemented more easily, and within a shorter time-frame than genetic tools. However, they are still dependant on the protein's synthetic capacity and turnover rates and, therefore, result in gradual protein elimination, limiting their applicability to fast-paced mechanistic studies while allowing for the occurrence of adaptive mechanisms (**Natsume et al.**, 2017; **Pauli et al.**, 2008; **Piskadlo**, 2017; **Röth et al.**, 2019). RNAi is also limited by knock-down efficiency and is susceptible to off-target effects (**Campbell et al.**, 2016; **Rakhit et al.**, 2014).

In light of these limitations, post-translational control strategies, which act directly on POIs at the protein level, have become necessary tools to dissect protein function. The potential of such tools to act at a more time-efficient rate makes them particularly relevant for inactivation of POIs involved in highly dynamic biological processes, such as cell-cycle and division regulation, differentiation, or neural activity. The study of POIs required in fundamental pathways, such as those involved in early embryonic development, or household genes, also requires tools with high spatiotemporal resolution that can conditionally target specific proteins *in vivo*. As a result, conditional post-translational control strategies now constitute a broad and ever-expanding toolkit at researchers' disposal (**Röth et al.**, 2019).

Conditional protein control through trigger-responsive mechanisms

Conditional protein control has been achieved through a vast and diversified set of approaches. Herein, focus will be given to strategies for protein inactivation, although most of them can, and have been, used to activate, recruit, modulate or simply track/probe protein expression as well. These strategies were broadly sub-divided into non-degradative and degradative approaches, for which we developed a new tool under the scope of this thesis. To provide context, and facilitate comparison between techniques, a very brief, essentially mechanistic, overview will be made.

Non-degradative approaches to protein inactivation

Blockade by small molecule inhibitors

One of the simplest ways of inactivating a POI is by the addition of a small molecule that can bind its active or allosteric site, thus locking it and preventing its activity. This is particularly effective in the case of enzymes or receptors, which have tractable binding sites (**Bondeson et al.**, 2017). Such an approach can provide very fast inactivation of the POI (**Campbell et al.**, 2016; **Rakhit et al.**, 2014), albeit constrained by the efficient delivery, and perfusion of drug to the target protein.

However, this very simple drug-based approach is extremely limited, given that it depends on the specificity of the drug towards the target, and the vast majority of proteins' activity does not rely so much on targetable ligand binding, rendering them "undruggable". Furthermore, chemical blocking agents work on an occupancy-based model, which means that they are only able to inactivate the POI while bound to it. This usually requires the delivery of high doses of the drug, with the possibility of off-target binding and side-effect occurrence (**Banaszynski et al.**, 2006; **Bondeson et al.**, 2017; **Toure et al.**, 2016). Therefore, and despite its power in some specific research-contexts, simplistic drug-based blockade has been relegated mostly to therapeutic purposes, and other triggers have been explored as research-oriented tools (**Campbell et al.**, 2016).

Allostery

Allosteric protein control relies on altering the activity of the POI through conformational change of its structure. This can be achieved by fusing two different domains with mutually exclusive folding: the binding of a ligand to one of these domains induces a conformational change in the other domain, affecting its structural folding, and, consequently, its activity. Alternatively, a more modular approach can be used, by using responsive domains within the POI's structure, to induce intra-molecular interaction and assembly/disassembly events. These domains therefore can work as switches, and they can respond to several stimuli, such as ligand binding or light (**Harper**, 2003; **Rakhit et al.**, 2014).

Allosteric modulation can depend on a broad set of structural alterations, such as major changes in folding, domain caging/liberation or small changes in flexibility and site exposure, relying on in-depth knowledge of the POI structure. It involves genetic alteration of the POI and validation of the binding and insertion sites positions, linker lengths and structural alterations produced by the trigger. This optimisation is usually empirically-driven, although efforts have been made towards *in silico* prediction of modulation targets based on amino-acidic sequences and statistical analysis (**J. Lee et al.**, 2008; **Rakhit et al.**, 2014).

Recruitment to anchor-proteins or complexes

POI inactivation can be achieved by recruiting the protein to a different sub-cellular organelle/sub-compartment or by sequestering it within a complex, in order to affect its activity and ability to exert its function. This is achieved by promoting the association of the

POI with other components, such as anchor-proteins located in specific compartments (targeted mis-localisation) or multimerising proteins capable of forming aggregates, in which the POI becomes trapped (protein complex recruitment). Targeted mis-localisation, is limited to the inactivation of proteins whose function is known beforehand and that are restricted to specific localisations to exert their activity. Recruitment is usually achieved using one of two conditional stimuli: chemicals or light exposure. In both approaches, at least two dimerisation domains must be engineered beforehand to allow dimerisation upon the application of the stimulus, one into the POI, and the other into the recruiting protein, (**Campbell et al.**, 2016; **Rakhit et al.**, 2014)..

Chemically-triggered dimerisation depends on the addition of CIDs (**C**hemical **I**nducers of ***D***imerisation), which are small compounds that recognise and bind two separate protein domains simultaneously. Some notable examples include FK1012 (the first natural CID) or rapamycin (an immunosuppressant drug and one of the most well-established heterodimeriser systems) (**Campbell et al.**, 2016; **Rakhit et al.**, 2014). Although CIDs can present nanomolar affinities towards their ligands, making it theoretically possible to inactivate the POI with high specificity and efficiency, temporal control of protein interference is limited by CID kinetics of uptake and distribution, often lacking tissue specificity. Furthermore, CIDs are often expensive, hard to synthesise, and can be very toxic even at very small doses (which is the case of rapamycin, for example). Many of them can also promiscuously bind other endogenous ligands, leading to off-target effects and/or competition between the POI and other CID-binding proteins in the cell. Finally, their nanomolar high affinity towards their ligands renders reversibility complicated, as it would usually require the addition of large amounts of a competing, high-affinity second-ligand to the system (**Campbell et al.**, 2016; **Kennedy et al.**, 2010; **Rakhit et al.**, 2014).

Alternatively, light-induced association relies on the existence of naturally photosensitive protein domains that dimerise when exposed to certain wavelengths (photoswitcheable domains). The use of light to induce protein association will be discussed in more detail ahead, in a sub-chapter on optogenetics.

Protein cleavage

Proteases that recognise specific target sequences, initially used for tag removal *in vitro*, represent a desirable strategy for precise targeted cleavage of POIs into inactive peptidic fragments. Viral proteins are particularly specific and efficient at stringently recognising target sequences with reduced off-target effects, behaving as proteic equivalents of DNA restriction enzymes (**Cesaratto et al.**, 2016).

One paradigmatic example of such proteins is the **T**obacco **E**tch **V**irus **p**rotease (TEVp), a C4 peptidase that recognises a 7 amino acids-long motif. Conditional cleavage can be achieved by engineering this motif within the POI sequence, thus creating TEVp-sensitive POIs. Subsequent introduction of TEVp into the system can be achieved either by direct addition to the medium or via genetic encoding under conditional promoters. TEVp has proven to be useful in *Drosophila melanogaster* studies involving mitotic proteins, namely in the

dissection of cohesin functions by conditional TEVp-mediated cleavage of one of its subunits (**Pauli et al.**, 2008).

Despite presenting a desirably high degree of specificity, TEVp cleavage requires the genetic alteration of the POI to insert the target sequence, and so prior knowledge of the protein's structure is important to identify sites whose alteration does not affect protein function and that are exposed enough to enable TEVp access (**Cesaratto et al.**, 2016; **Piskadlo**, 2017). Furthermore, direct injection of TEVp into the tissue of interest is not always possible, which can significantly limit its application in some contexts due to slow rates of POI elimination.

Stability disruptive approaches to protein inactivation

General considerations on endogenous protein degradation mechanisms

Most protein degradation tools rely on the use of the endogenous cellular machinery naturally involved in protein turnover, in which **ub**iquitin (Ub) plays a central role.

Ub is a small protein, whose conjugation with a target protein, or ubiquitination, has a variety of tightly regulated functions within the cell. Briefly, ubiquitination of a substrate follows a sequential process in which Ub is firstly activated by forming a high-energy bond with an ubiquitin-activating enzyme (E1). The E1 then transfers the activated Ub to an ubiquitin-conjugating enzyme (E2). Finally, an ubiquitin-ligase enzyme (E3) allows the transfer of Ub to the substrate by formation of an isopeptide bond. Further Ub moieties can then be added (poly-ubiquitination) to form Ub-chains, and, conversely, Ub signals can be removed or trimmed by de-ubiquitination enzymes (**Akutsu et al.**, 2016; **Hicke et al.**, 2003a). Distinct cellular functions are associated with: different E2-E3-substrate interactions; the position and type of residues involved in the interactions between Ub, E2, E3 and the substrate; size, position and modifications of the Ub chains; and the balance between ubiquitination and de-ubiquitination. Taken together, these aspects control the fate of the modified substrates, regulating a variety of cellular processes, such as cell cycle, protein sorting and trafficking, DNA repair and inflammation signalling (**Akutsu et al.**, 2016; **Anandapadamanaban et al.**, 2019; **Dammer et al.**, 2011; **Hicke et al.**, 2003b).

One of the main and better-studied events mediated by ubiquitination is protein targeting for degradation, particularly through the so-called **U**biquitin-**P**roteasome **S**ystem (UPS). This requires the substrate to be modified with a lysine-48 Ub-chain (Ub-^{48}Ub chain, or canonical Ub chain), which targets it to the 26S proteasome, a multimeric protein complex with regulated protease activity, where misfolded or damaged proteins are unfolded and undergo controlled recycling (**Akutsu et al.**, 2016; **Röth et al.**, 2019). Ub has also been associated with alternative degradation pathways, such as the autophagy/lysosomal system, or the endoplasmic reticulum associated degradation in yeast (**Dammer et al.**, 2011; **Xu et al.**, 2009).

In general, tools for the conditional control at protein level rely on the recruitment of the POI to an E3, so that it is ubiquitinated and subsequently degraded (**Röth et al.**, 2019). This recruitment can either be achieved by genetically fusing controllable domains to the POI (degron-mediated recruitment), or by introduction of a molecule with the ability of binding the POI with high-affinity, and subsequently destabilising it.

Degron-mediated recruitment

Degrons are small instability-inducer domains, which can be genetically fused to a POI to condition its targeting to the proteasome. They can be activated by different stimuli, such as temperature, small molecules, light or the expression of other proteins (**Röth et al.**, 2019).

The first conditional degron to induce proteolysis of a POI was described for budding yeast, and made use of a ubiquitin-proteasome pathway termed N-end rule (**Campbell et al.**, 2016). The N-end rule states that the identity of the N-terminal residue of a protein can determine its half-life (**Hochstrasser**, 1996), and that some N-terminus residues induce protein de-stabilisation by targeting it for ubiquitnation. Conditional degradation was achieved by fusing the POI to an N-degron derived from a temperature sensitive protein, dihydrofolate reductase (DHFR), engineered to present a hidden de-stabilising residue (Arg, in this case) (**Banaszynski et al.**, 2006). A temperature shift from 24°C to 37°C leads to the unfolding of the degron, thereby exposing the Arg residue at its N-terminal, inducing POI poly-ubiquitination (**Natsume et al.**, 2017). This system is able to induce rapid POI degradation, but is greatly limited in application by the need for a very drastic temperature shift, which is incompatible, for example, with mammalian cell culture. It is also restricted to proteins that retain function upon N-terminal fusion of the degron (**Campbell et al.**, 2016).

To avoid drastic temperature shifts, the use of small molecules to induce conditional degrons was explored and is currently the predominant type of degron system (**Natsume et al.**, 2017). One important approach based on small molecules is the use of conditionally stable systems that rely on destabilising domains (DDs). DDs are constitutively destabilising degrons that can be stabilised in the presence of a small molecule ligand. POIs modified by fusion with a DD are subsequently degraded upon ligand removal from the system (**Maynard-Smith et al.**, 2007). Two examples of DD/ligand pairs include FKBP12/Shield-1 and UnaG/bilirubin, both derived from the FKBP12/rapamycin/mTOR kinase complex (**Natsume et al.**, 2017). One drawback of DD systems is that they require constant ligand presence to preserve protein function (**Hörner et al.**, 2012). To circumvent this, a follow-up study from the authors of the FKBP12/Shield-1 system reports the application of the same ligand in an alternative approach that is opposite of the DD technology (**Bonger et al.**, 2011). In this study, the authors describe a domain, which they named LID (Ligand Induced Degradation), that is composed of a hidden degron. Shield-1 addition to the system causes a conformational alteration that exposes the LID degron, and elicits POI degradation (**Bonger et al.**, 2011).

Asides from DDs, one of the most well-established examples of small-molecule induced degrons is the auxin-inducible degron (AID), derived from a plant natural degradation system. In this case, the E3 ligase is a highly conserved ubiquitin ligase complex, SKP1/CUL1/F-Box (SCF), which is present in both plant and non-plant eukaryotic cells. Upon expression of a plant F-box protein (TIR1), POIs bearing the AID motif can be recruited to this complex by addition of hormones from the auxin family, such as Indole 3 Acetic Acid (IAA). The SCF then catalyses POI ubiquitination and subsequent degradation (**Bondeson et al.**, 2017). This degron has been applied to many systems, including human, chicken, mouse and yeast-derived cell lines (**Natsume et al.**, 2017). Notably, AiD has been used in conditional targeted depletion of Nanos and Vasa, two highly pleiotropic maternal effect proteins in the *Drosophila* female germline, for the study of oogenesis mechanisms (**Bence et al.**, 2017). Despite its potential, AiD requires the expression of exogenous TIR1 in these systems, and depends on the delivery of relatively large amounts of IAA (**Röth et al.**, 2019).

Regardless of the activation stimulus, degron use always requires POI genetic alteration, and several iterations in design are usually necessary to obtain optimal degrons for each protein (**Campbell et al.**, 2016).

High affinity binder mediated recruitment

Alternatively to degrons, there is a number of tools that recruit POIs to the proteasome by the addition of high affinity binders (**Röth et al.**, 2019).

Proteolysis-targeting chimeras (PROTACs) are small heterobifunctional molecules that have two discrete recruiting ligands connected by a chemical linker. One ligand is specific for the POI, and the other recruits an E3 ligase (**Bondeson et al.**, 2017). Thus, PROTACS form ternary complexes, positioning the POI in a position that favours E3-ligase mediated polyubiquitination (**Toure et al.**, 2016). These systems do not require prior genetic modification of the POI, and have been able to target the degradation of many proteins that had been considered "undrugabble" by small-molecule inhibitors (**Röth et al.**, 2019; **Toure et al.**, 2016). However, they present very limited potency, requiring relatively high concentrations, induce only partial POI degradation, and they are often cell impermeable (**Bondeson et al.**, 2017). PROTACs also require extensive individual optimisation. For example, linker optimisation poses a significant challenge to PROTACs efficiency (**Toure et al.**, 2016). Finally, they require empirical determination of the best ligase for each POI and the employment of highly selective small molecule protein binders, whose development is resource and time-intensive, which limits their application to most endogenous POIs (**Fisher et al.**, 2018).

The specificity limitations presented by PROTACs and other small molecule degraders drove the development of systems that recognise POIs by targeting not the POIs *per se*, but through common tags, employed, for example, in protein purification (such as the HaloTag) or in imaging (such as GFP) (**Röth et al.**, 2019). Because tagged fusion versions of most POIs are usually available, or at least easy to obtain, targeting such tags enables the creation of

more generalisable degradation systems, without the need for further POI genetic modification (**Campbell et al.**, 2016; **Natsume et al.**, 2017).

In particular, the use of fluorescence tag proteins as targets for proteasomal degradation has the added advantage of enabling live tracking of the depletion process. Notably, two similar systems that recognise GFP-tagged POIs have been described: DeGradFP, and AdPROM (**Röth et al.**, 2019). Both of them target POIs for degradation by recruiting them to an endogenous E3 ubiquitin ligase complex, CUL, which possesses an E3 ligase bound to a selective adaptor. Different CULs posses different adaptors, which recognise specific substrate-receptors (**Fulcher et al.**, 2016). For each system, recruitment was achieved by the introduction of an anti-GFP nanobody fused to a receptor able to interact with the CUL adaptor subunit (**Caussinus et al.**, 2012; **Fulcher et al.**, 2016). The nanobody binds the GFP-tagged POI with high-affinity and targets it to the CUL complex for subsequent degradation.

Recently, Daniel et al. have reported the combination of the anti-GFP nanobody approach with the classical auxin degradation system to create an AID-nanobody for GFP-tagged POI degradation (**Daniel et al.**, 2018). The authors compared their system to DeGradFP in terms of their ability to induce triggered degradation of the anaphase promoting complex subunit (ANAPC4). The auxin-dependent nanobody enabled a much more refined temporal control than DeGradFP for this POI, with tagged-ANAPC4 being efficiently targeted for degradation within 3h of auxin addition.

Taken together, these systems clearly highlight an increasing tendency towards the development of highly generalisable tools that minimise the need for POI genetic alterations, while at the same time allowing tight temporal control and live tracking of the POI depletion.

Project background and aims

The new tool developed in this thesis essentially builds upon two systems used for conditional protein control: an optogenetic tool, called **L**ight **A**ctivated **R**eversible **I**nhibition by **A**ssembled **T**rap (LARIAT, (**S. Lee et al.**, 2014)), and an E3 ligase-based method of endogenous degradation, called Trim-away (**Clift et al.**, 2017). Relevant aspects of optogenetics will be discussed, and both systems will be presented in-depth.

Optogenetics

The limitations associated with CIDs use have led to the use of light as an alternative trigger to control protein function. The first photoswitches used in light-based systems were naturally occurring photoreceptor proteins, which regulate light-dependant processes, in many different organisms, such as plant development or circadian rhythm. Via photon absorption, these proteins exist in equilibrium between conformationally different active and inactive states, which are modulated by intra- and/or intermolecular interactions associated with photon absorption (**Klewer et al.**, 2019).

There is a variety of photoswitches that can mediate homo or heterodimerisation, and they can respond to a variety of wavelengths. For example, UVR8 and CBD both homodimerise in the dark and dissociate upon UV, or green light exposure, respectively (**Klewer et al.**, 2019); phytochrome PhyB (*Arabidopsis thaliana*) homodimerises when active and heterodimerises with different partners when inactive, forming multimeric complexes (**Hörner et al.**, 2012). Recently, a large-scale online annotated database called OptoBase has been created to cover the diversity and versatility of these optogenetic switches (**Kolar et al.**, 2018), which clearly highlights the growing interest and potential in this field.

Advantages and limitations of light based systems

Many photoswitcheable proteins use wavelengths that usually fall within the range of fluorescent imaging, lowering the risk for phototoxicity, and enabling application to *in vivo* studies (**Klewer et al.**, 2019). Live imaging protocols of acquisition can simultaneously serve as triggered activation, avoiding extra activation steps and rendering the system more compact. Moreover, light-based systems bypass perfusion limitations, medium changes, and have low potential for off-target or toxic effects associated with exogenous molecules (**Campbell et al.**, 2016; **Rakhit et al.**, 2014). Activation at different wavelengths broadens the choice range for different applications. For example, red light activated switches can be a more desirable choice in deep tissue samples because bigger wavelengths penetrate more efficiently (**Klewer et al.**, 2019).

However, light-based approaches also present limitations. High spatial resolution via targeted light beams often requires the use of very specialised microscopes and software (**Campbell et al.**, 2016). Some photoswitches rely on continuous or repeated light stimulus that can cause phototoxicity or local heating. Furthermore, the introduction of chromophores derived from plants and bacteria into animal systems may lead to fluorescent background (**Klewer et al.**, 2019; **Rakhit et al.**, 2014).

LARIAT

The **cry**ptochrome-2 (CRY2)-CIB1 system is derived from *A. thaliana*, and was initially described by Kennedy et al. in 2010. Upon blue-light (450nm) exposure, CRY2 becomes activated and reversibly binds **c**ryptochrome **i**nteracting **b**HLH (CIB1) within seconds, with no need for exogenous chromophore presence. CRY2 interacts with CIB1 through CIB1's N-terminal, 170 first amino acids (denoted CIBN) (**Kennedy et al.**, 2010). Later on, Lee at al. took advantage of this system and expanded it into a modular tool for inactivating proteins via aggregation which they called **L**ight **A**ctivated **R**eversible **I**nhibition by **A**ssembled **T**rap (LARIAT). LARIAT consists of two modules: a light induced dimeriser, and a multimeric protein complex (**S. Lee et al.**, 2014).

The light-induced dimeriser acts both as the photo-switch of the system and as the module for protein recruitment, by fusion of CRY2 to a single domain camelid-derived antibody (V_HH or nanobody). V_HH binds the common green fluorescent protein (GFP) fusion tag with high specificity, allowing for the versatile recruitment of any GFP-tagged POI (**Rothbauer et al.**, 2006). The multimerisation protein complex enables the formation of high order

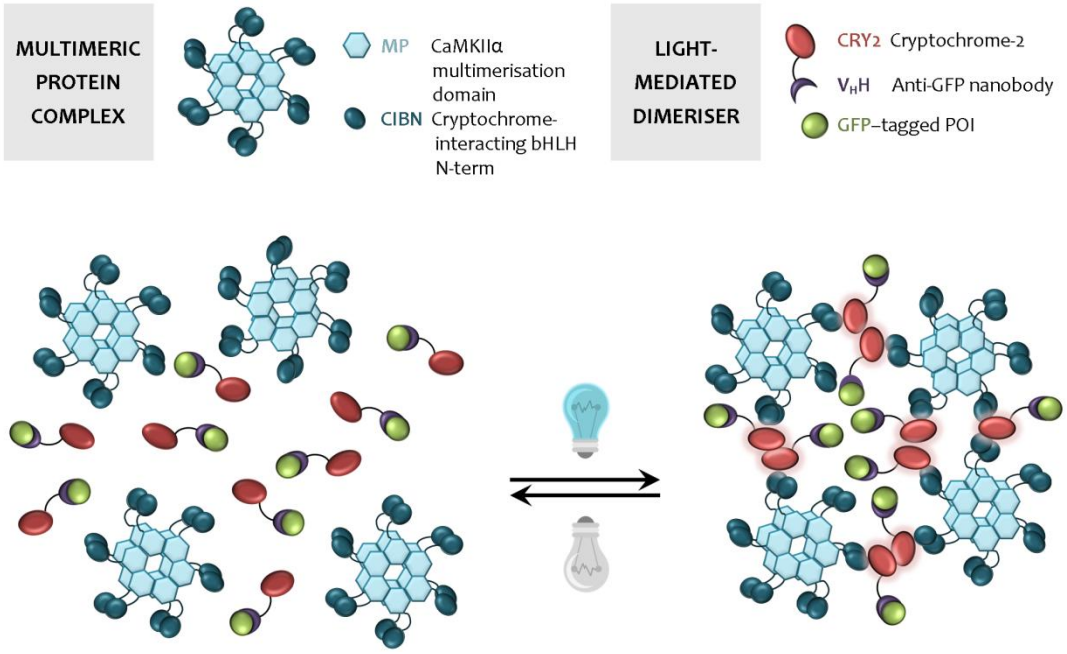

Figure 1. Schematic representation of light–activated reversible inhibition by assembled trap (LARIAT)

Cryptochrome-interacting bHLH N-terminal (CIBN) fused with the multimerisation domain from CaMKIIα (MP) forms dodecamers in the cytoplasm. Cryptochrome-2 (CRY2) is fused with an anti-GFP nanobody that specifically binds to GFP-tagged proteins. Blue light (450nm) triggers CRY2 activation, oligomerisation, and binding to CIBN, eliciting the formation of clusters that trap GFP-tagged proteins. Upon the removal of the light stimulus, CRY2 spontaneously reverts to its ground inactivated state and the clusters disassemble.

[Adapted from Osswald et al. (2019)]

complexes, or clusters. At its core lies a **M**ultimeric **P**rotein (MP), derived from the C-terminal of Ca^{2+}/calmodulin-dependent protein kinase IIα (CaMKIIα), which spontaneously self-assembles into a 12 subunit oligomer in the cytoplasm. The MP is fused to CIB1, thereby associating with the photoswitcheable dimeriser, to generate a light-inducible clustering tool (Figure 1, (**S. Lee et al.**, 2014)).

The authors of the LARIAT system were able to recruit GFP-tagged guanine nucleotide exchange factor (VAV2) into light-induced clusters in a murine cell line. Vav2 induces membrane protusion, and VAV2 light-triggered trapping elicited membrane retraction within few minutes. LARIAT also proved effective at inhibiting microtubule function during mitosis by clustering GFP-tubulin (**S. Lee et al.**, 2014). LARIAT authors have since further characterised the parameters that drive CRY2 oligomerisation efficiency, and have identified a short peptide called Clust which improved the kinetics of CRY2 homodimerisation and enabled the formation of large CRY2 clusters (**Park et al.**, 2017). This would therefore bypass the need of incorporating a CIBN-multimerisation module for light-induced clustering.

Our group has introduced LARIAT technology in *D. Melanogaster* S2 cells. In particular, it was shown that light-induced clustering can inactivate the mitotic kinase MpsI, and disrupt the membrane localisation of the polarity regulator lethal giant larva (Lgl) (**Osswald et al.**, 2019). We were further able to use this tool to probe protein-protein interactions, as will be described in CHAPTER IV.

E3-ligase mediated conditionally induced degradation

TRIM21 – a unique player at the last line of immunological defence

Tripartite **M**otif-containing protein **21** (TRIM21), also known as Ro52, was initially described in the context of autoimmune disorders such as Sjörgren's syndrome, rheumatoid arthritis, and systemic lupus erythematosus. For decades, the presence of circulating auto-antibodies against TRIM21s in these patients was used for diagnosis purposes, but the protein's function remained unknown (**Foss et al.**, 2015; **Keeble et al.**, 2008). Structural characterisation of TRIM21 subdomains has since shed light on its function, namely through the identification of an N-terminal motif that places it in the TRIM family (**Oke et al.**, 2012), a group of proteins which mediate innate immune response, amongst other critical cellular functions (**Keeble et al.**, 2008).

TRIM21 is uniquely expressed in almost all tissues of mammalian cells (**Fletcher et al.**, 2016). It is localised essentially in the cytosol (**Espinosa et al.**, 2006), where it acts as a last line of defence molecule, by intercepting cytoplasmic antibody-coated (opsonised) viral pathogens that have escaped extracellular mechanisms of immunity (**Mallery et al.**, 2010). Current knowledge of the mechanism of action of this receptor in innate immunity is summarised in Figure 2. TRIM21 has an exceptionally broad receptor ability and is able to recognise and bind the Fc portion of IgA, IgM, and all subclasses of IgG antibodies with high affinity (**James et al.**, 2007; **Keeble et al.**, 2008). In the presence of cytosolic Ab:substrate complexes, TRIM21 promptly dimerises, and binds opsonising Abs through their Fc portions in a preferential 1:2 Fc:TRIM21 ratio (**Keeble et al.**, 2008; **Mallery et al.**, 2010). After Ab binding, TRIM21 undergoes auto-ubiquitination by interaction with E2 conjugating enzymes (**Espinosa et al.**, 2006; **Fletcher et al.**, 2015), which culminates in proteasome recruitment and elicits rapid degradation of both substrate and Ab (**Mallery et al.**, 2010).

Importantly, the mechanism of proteasomal recruitment is not yet fully understood. TRIM21-mediated viral degradation was found to be strictly dependent of AAA+ ATPase v97/VCP, a multi-domain complex that interacts directly with poly-Ub chains and is capable of extraction and unfolding of proteins from larger complexes, suggesting a possible role in pre-proteasomal substrate disassembly (**Foss et al.**, 2015). A uniquely complex mechanism of sequential ubiquitination using anchored, non canonical, Ub-^{63}Ub chains as a precursor was also found to be required for proteasomal targeting (**Fletcher et al.**, 2015).

Apart from this anti-viral neutralising role, TRIM21 also initiates a synchronous immune signalling cascade through transcriptional up-regulation of inflammatory cytokines (**Fletcher et al.**, 2015; **Foss et al.**, 2015), and activates several signal transduction pathways (**Fletcher et al.**, 2016).

Notably, human TRIM21 is able to catalyse the formation of both canonical Ub-^{48}Ub and non-canonical Ub-^{63}Ub chains, and has been described to interact with a variety of nuclear and cytosolic E2 conjugating enzymes, including UBE2D1-4, UBE2E1-2 (**Espinosa et al.**, 2011), UBE2E1 (**Anandapadamanaban et al.**, 2019), UBE2w, and also the heterodimer

UBE2N/UBE2V2, as well as with de-ubiquitinase Pho1 (**Fletcher et al.**, 2015). TRIM21 can also translocate to the nucleus upon certain pro-inflammatory conditions (**Oke et al.**, 2012).

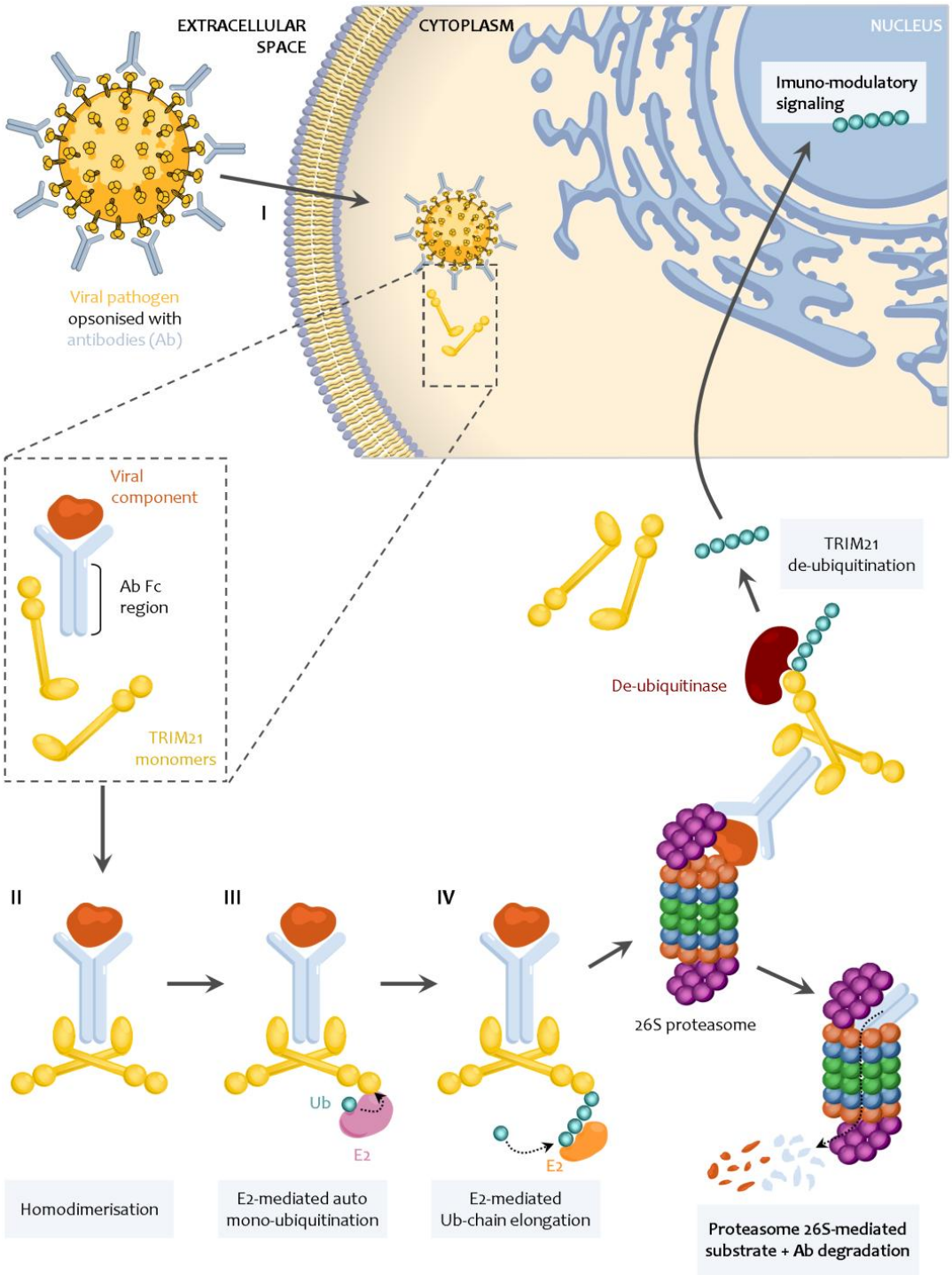

Figure 2. TRIM21 endogenous functions in immune response to Ab:pathogen complexes

TRIM21 acts as a last-line of defence against Ab opsonised pathogens that have escaped extracellular immunological control and (I) entered the cell. (II) TRIM21 monomers recognise and bind the Fc-portion of opsonising antibodies. (III) TRIM21 then acts as an E3-ligase and undergoes E2-mediated mono-ubiquitination, and (IV) subsequent anchored Ub chain elongation, which enables rapid 26S proteasome recruitment of the entire complex, by a mechanism not yet fully described. Viral neutralisation is achieved through viral substrate and Ab proteasome 26S-mediated degradation, before the virus has time to replicate. Simultaneously, TRIM21 is de-ubiquitinated, eliciting nuclear activation of pro-inflammatory transcription factor pathways, that signal neighbouring cells and contain the infection.

Taken together, these findings highlight the versatility of this unique receptor, and its importance in providing an early warning of otherwise undetected pathogen exposure, and eliciting a rapid degradation-mediated anti-viral response (**Fletcher et al.**, 2016).

TRIM21 structural subdomains

TRIM21 structural understanding has been key to unveil its functions in innate immunity. The protein presents an RBCC N-terminal motif, which is a feature of the TRIM family, and is composed of: a RING (Really Interesting New Gene) domain, followed by a type 2 B-Box and a Coiled Coil (CC) domain (**Oke et al.**, 2012). TRIM21's uniquely broad receptor ability is conferred by a C-terminal PRYSPRY domain, which is responsible for the recognition and high affinity binding to the Fc portion of Ab heavy chains (**Foss et al.**, 2015; **Keeble et al.**, 2008). TRIM21 subdomains and their respective functions are depicted in Figure 3.

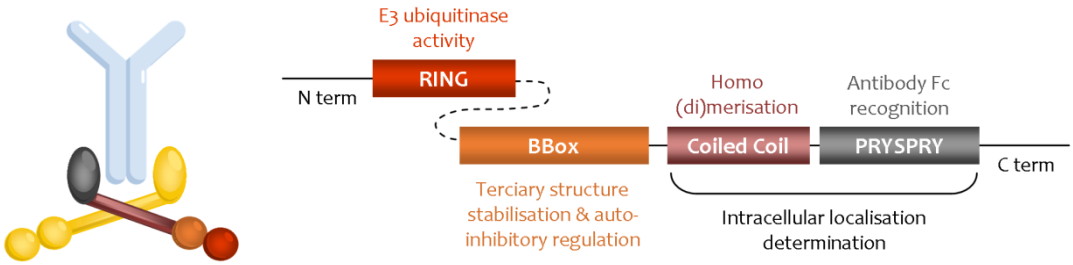

Figure 3. Schematic representation of the TRIM21 protein domains

Dimerised TRIM21 bound to an Ab (light blue) is depicted on the left, with a corresponding colour coded-depiction of TRIM21 subdomains on the right. Each TRIM21 monomer (yellow) is composed of an N-terminal RBCC motif and a C-terminal PRYSPRY domain (grey) responsible for Ab recognition and binding. The RBCC motif includes an E3 ligase RING domain (red), followed by a regulatory B-Box (orange) and a dimerising-mediator Coiled Coiled (CC) domain (plum). Both the CC and the PRYSPRY domains also influence nuclear *vs* cytosolical localisation [Domains are not to scale.]

Like many proteins in the TRIM family, the ubiquitinase activity of TRIM21 is RING dependent (**Espinosa et al.**, 2006). In fact, the isolated RING domain of TRIM21 is able to form Ub chains within minutes, constituting a highly-active E3 ligase (**Dickson et al.**, 2018). Very recently, the crystal structure of the RING domain in complex with human E2-conjugating UBE2E1 enzyme was reported, and Lys residue 61 was identified as the primary site for TRIM21 E2-mediated auto-ubiquitination (**Anandapadamanaban et al.**, 2019). The BBox domain is a Zinc-binding entity that was found to stabilise the tertiary structure of the whole protein, but whose function is not yet completely understood (**Wallenhammar et al.**, 2017). Recently, the BBox was found to occupy the E2 binding site on RING, hence having an auto-inhibitory function that sterically regulates TRIM21's activity. Phosphorylation of the serine residue at position 80 in the RING domain by kinases IKKb and TBK1 acts as a switch that relieves B-Box inhibition, and activates the protein (**Dickson et al.**, 2018). The CC-domain is generally involved in the oligomerisation of RBCC-containing proteins and it is necessary for TRIM21 dimer formation, which is the preferred state for the protein, enabling simultaneous engagement of both Ab heavy chains (**Mallery et al.**, 2010). Importantly, and unlike other TRIM proteins, it has recently been shown that, despite this, dimer formation is not intrinsically required for TRIM21 activity (**Dickson et al.**, 2018). Furthermore, the CC-

domain, together with the C-terminal PRYSPRY domain, is also important in determining the cytoplasmic *vs* nuclear localisation of the protein (**Oke et al.**, 2012).

Keeble et al. have found that TRIM21 is a structurally conserved protein amongst mammals and the binding sites on both TRIM21 and Fc support interchangeable IgG recognition and binding between murine, canine, primate, and human species (**Keeble et al.**, 2008). These authors also report considerable homology between human and mouse TRIM21, which is supported by the resolved 3D structures of the murine TRIM21 PRYSPRY domain, both free and in complex with murine Fc. However, contrary to human TRIM21, whose RING and BBox domains have been resolved and are relatively well characterised (**Anandapadamanaban et al.**, 2019; **James et al.**, 2007; **Wallenhammar et al.**, 2017), not many studies have focused on the RBCC motif in *Mus musculus*. Espinosa et al. have shown that the mouse RING domain is necessary for TRIM21-mediated regulation of proliferation and cell death in the context of viral infection (**Espinosa et al.**, 2006), but the E3 activity of mouse RING and ubiquitination states remain uncharacterised.

Repurposing TRIM21 for conditional protein depletion: the Trim-Away system

Dean Clift et al. have established a method that harnesses TRIM21 Ab recognition ability, combined with endogenous UPS machinery to achieve post-translational endogenous protein depletion, which was named "Trim-Away" (**Clift et al.**, 2017). The authors describe their tool as a 3-step strategy, starting with the introduction of exogenous TRIM21 in the cells of interest. After that, an antibody against the POI must be delivered to the cells. Thirdly, TRIM21 mediates ubiquitination and proteasome degradation of the antibody-bound POI.

As a proof of concept, they used a GFP-specific antibody to target GFP for degradation, in different intracellular regions. In TRIM21 over-expressing mouse oocytes, Trim-away was able to deplete membrane-anchored GFP and nuclear GFP, containing a nuclear localisation signal, upon microinjection of the anti-GFP Ab.

Despite its potential, the heavy dependence of Trim-Away on Abs poses limitations to this system. Introducing large amounts of pure and highly selective IgG antibodies into target cells is not only challenging, but extremely costly and therefore not suitable for large-scale applications (**Röth et al.**, 2019). Moreover, and even though the authors of the system propose an electroporation protocol to allow bulk-cell population studies, Trim-Away is still not applicable to live organisms. Another limitation comes from the inability of Abs to reach POIs in certain cellular compartments, which the authors report themselves. For instance, effective depletion of GFP fused to histone-H2B (H2B-GFP), and a subset of protein kinase mTOR, was hindered due to Ab inaccessibility. In the case of H2B-GFP, the authors circumvented this issue by creating a chimeric Fc-nanobody. To this purpose, they had to fuse the Fc-domain of an Ab to an anti-GFP nanobody, to obtain an Fc-nanobody whose size was compatible with nuclear penetration. Another aspect to consider is that Ab introduction in mammalian systems followed by interaction with a signalling agent such as

TRIM21 could create an artificial infection-like state, which can limit Trim-Away application to any systems that study immune-regulatory pathways.

However, the results obtained with the Trim-Away system clearly highlighted the potential for TRIM21 to be used as a post-translational conditional tool with very rapid depletion kinetics. For example, cohesion protein complex member Rec8, which mediates sister cromatid cohesion, was degraded within an average of 11 min, which was sufficient to rapidly elicit sister cromatid separation (**Clift et al.**, 2017). Not only is this remarkable as an application of TRIM-21 to the highly dynamic process of cell division, Rec8 is also a good example of the need for protein interference at the post-translational level. In fact, Rec8 does not turnover, and therefore its genetic and or RNAi-mediated depletion are particularly challenging. Depletion of several endogenous substrates, such as centrosomal protein pericentrin or microtubule motor protein Eg5, was achieved within hours, or even minutes upon Ab injection, respectively, using Trim-away. Trim-Away proved to be applicable to both murine and human cells lines, and mouse oocytes. The authors also used Trim-Away to impact signalling pathways through selective degradation in common human cell lines. Interestingly, they found that some cell lines, such as HeLa, were able to partially degrade the POI ERK1 kinase upon delivery of anti-ERK1 Ab alone, by making use of their endogenous pool of TRIM21. Regardless, the delivery of exogenous TRIM21 improved the depletion efficiency in all cell lines.

The main purpose of this thesis was to build upon these results that suggest TRIM21 ability to mediate targeted protein degradation, but using a light-based, optogenetic tool as a trigger, by-passing the need for Ab delivery. The fact that both techniques possess rapid temporal response is particularly adequate for application to the study of highly dynamic processes.

▪ Blank page ▪

CHAPTER II

Materials and methods

▪ Blank page ▪

Molecular biology

pHW-CIBN-MP_RW-CRY2-V_HH (Supplementary Figure 1), pHW-CIBN-MP_pH-CRY2-V_HH, pHGW-aPKC, pHGW-aPKCdN and Ed-GFP (used in CHAPTER IV) have been previously described (**Johnston et al.**, 2009; **Osswald et al.**, 2019). Figure 4 depicts all of these constructs, as well as the eleven original constructs produced within the context of this thesis, together with the name with which they will be termed throughout the text.

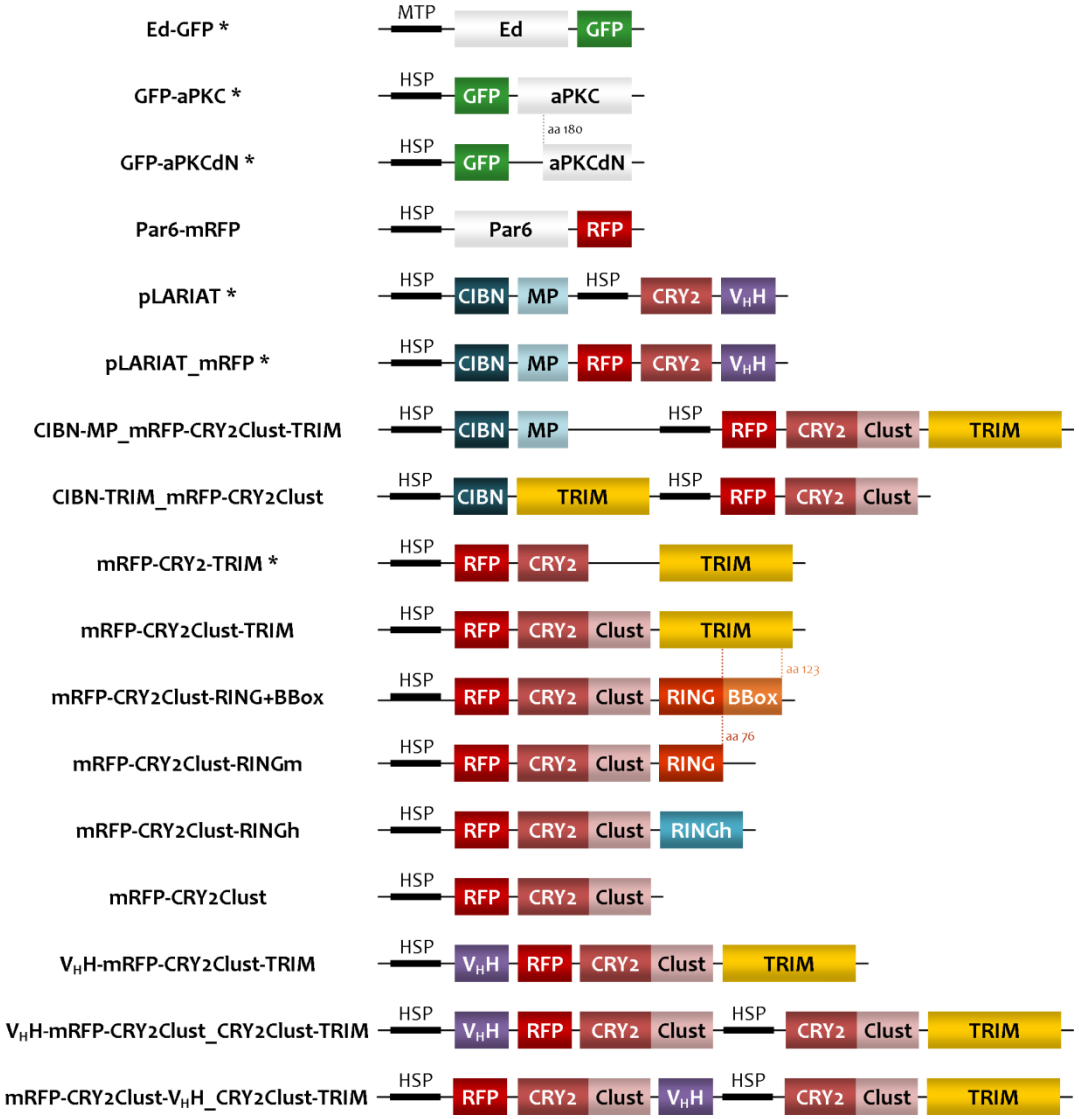

Figure 4. Construct listing and schematic depiction of domains.

Each line corresponds to a single construct (name on the left). Domain lengths are not to scale. Clust sequence is fused C-terminally to CRY2 in all Clust-containing constructs. Asterisks indicate constructs that were not cloned by the author (original descriptions are referenced throughout the text). Dashed lines symbolise truncation positions of full aPKC to generate aPKCdN (aa 180-606) and of full TRIM to produce RING+BBox (aa 1-123) or RINGm (aa 1-76).

[aa = aminoacid; MTP = Metallothionein promoter; HSP = Hsp70 promoter; TRIM = mouse TRIM21 (full)]

The steps for obtaining each expression vector are summarily outlined below. All constructs were cloned into *Drosophila* Gateway modules (Life Technologies). General template destruction was performed using DpnI restriction enzyme (New England Biolabs). All PCR

amplifications were done using Phusion High Fidelity DNA polymerase (New England Biolabs). Recombination into expression vectors was done through LR Clonase II (Thermo Fisher Scientific)-mediated recombination. Chemically competent TOP10 *Escherichia Coli* were used in all transformations. All expression vectors were sequenced prior to transfection.

The Clust peptide, as described by Park and colleagues (**Park et al.**, 2017), was optimised for *Drosophila* expression and its sequence (5' – GCCCGCGATCCCCCCGATCTGGATAAC – 3') is common to all Clust-containing constructs. Except when clearly stated otherwise, 'TRIM' refers to the mouse TRIM21 cDNA sequence (kindly provided by Liam Cheesman, and available as Trim21-201, Ensemble Genome Database Project, rs31986801 and rs32470326)

Cloning of plasmids for expressions in S2 cells

mRFP-CRY2Clust-TRIM: To obtain a pENTR-CRY2Clust plasmid, Clust's sequence was encoded into two partially complementary primers (*Cry2Clust Fw* and *Cry2Clust Rev*, Table 1), which were used to amplify a pENTR-CRY2-TRIM plasmid (generated by Mariana Osswald) by PCR. The template was then destroyed, and the PCR product was used to transform competent bacteria. Recombination into a pHRW plasmid was then used to obtain a pHRW-CRY2Clust-TRIM.

mRFP-CRY2Clust, mRFP-CRY2Clust-RING+BBox and mRFP-CRY2Clust-RINGm: pHRW-CRY2Clust, pHRW-CRY2Clust-RING+BBox, and pHRW-CRY2Clust-RINGm were all obtained by PCR amplification of pHRW-CRY2Clust-TRIM using primers *pENTR Fw* and either *Clust linker Rev*, *BBox clon CT Rev* or *RINGm Rev* (Table 1), respectively. Templates were then destroyed, and each PCR product was used to transform competent bacteria.

mRFP-CRY2Clust-RINGh: To obtain a pENTR-CRY2Clust RINGh vector, the human RING domain (RINGh, amino acids 1-84) was amplified from a human TRIM21-containing pGEMHE-mCherry-hTRIM21 plasmid (kindly provided by Dean Clift) by PCR, using primers *TRIMh for pENTR Fw* and *RINGh Rev* (Table 1). The pENTR-CRY2Clust vector was amplified from pENTR-CRY2Clust-TRIM using primers *pENTR Fw* and *Clust linker Rev* (Table 1). The PCR products were mixed, and, after template destruction, used to transform competent bacteria to generate pENTR-CRY2Clust-RINGh. Recombination into a pHRW plasmid was then used to obtain pHWR-CRY2Clust-RINGh.

V_HH-mRFP-CRY2Clust-TRIM: V_HH was amplified from pENTR-CRY2-V_HH (previously described in (**Osswald et al.**, 2019)), using primers *VHH for HSP Cterm Fw* and *VHH link RFP Rev* (Table 1). pHRW-CRY2Clust-TRIM was amplified by PCR using primers *VHH link RFP Fw* and *HSP link Rev* (Table 1) to generate a PCR product with terminal regions homologous to those of the insert PCR. Insert and PCR products were mixed and, after template destruction, the mix was used to transform competent bacteria and obtain a pH-V_HH-RW-CRY2Clust-TRIM expression vector.

Par6-mRFP: pHWR-Par6 cloning has been previously described (Osswald et al., 2019). Briefly, the Par6 sequence was amplified from its complementary DNA (Berkeley *Drosophila*

Genome Project (BDGP) Gold collection), using primers *Par6 Fw* and *Par6 Rev* and the insert PCR product was mixed with pENTR vector PCR product (obtained using primers *pENTR Fw* and *pENTR Rev*). After template destruction, the mix was used to transform competent bacteria. Recombination into a pHWR plasmid was then used to obtain pHWR-Par6.

Double expression vector obtention

To generate double promoter constructs joined in the same expression vector, expression vectors containing an additional AfeI restriction site before the Hsp70 promoter were used. The AfeI site had been inserted using site-directed mutagenesis, as described previously (**Osswald et al.**, 2019), to allow excision of expression cassettes. Herein, a '2GT' subscript notation will be used to denote all relevant plasmids described above in which this AfeI restriction site was present. Note that the expression cassettes are independent; the double construct's names were arbitrarily chosen out of convenience and do not necessarily reflect the two cassettes' positions relative to the origin of replication).

All gel purifications from gel were done using NucleoSpin® Gel and PCR Clean-up kit, according to manufacturer's instructions. All ligations were done in a 1:1 pDNA amount proportion using T4 DNA ligase (New England Biolabs).

CIBN-MP_mRFP-CRY2Clust-TRIM: The HRW-CRY2Clust-TRIM expression cassette was excised from p_{2GT}HRW-CRY2Clust-TRIM using Eco47III (AfeI equivalent, Thermo Fisher Scientific) and PvuI-HF (New England Biolabs). Parallel to this, pHW-CIBN-MP (described in (**Osswald et al.**, 2019)) was linearised with PvuI-HF (New England Biolabs) and PmeI (New England Biolabs). Fragments of interest from each double digestion were purified from gel, ligated and used to transform competent bacteria to obtain a pHW-CIBN-MP_HRW-CRY2Clust-TRIM double expression vector.

CIBN-TRIM_mRFP-CRY2Clust: Firstly, a pENTR-CIBN-TRIM plasmid was generated. To this purpose, TRIM was amplified and extended with an N-linker region by PCR from pHRW-CRY2Clust-TRIM using primers *TRIM Nlinker Fw* and *TRIM for pENTR Rev* (Table 1). pENTR-CIBN (previously described in (**Osswald et al.**, 2019)) was amplified by PCR using primers *pENTR Fw* and *CIBN-MP long linker Rev* (Table 1) to generate a PCR product with terminal regions homologous to those of the insert PCR. Insert and PCR products were mixed and, after template destruction, the mix was used to transform competent bacteria and obtain a pENTR-CIBN-TRIM vector. Recombination into a p_{2GT}HW plasmid generated a p_{2GT}HW-CIBN-TRIM expression vector. Then, the HW-CIBN-TRIM expression cassette was excised from p_{2GT}HW-CIBN-TRIM was using Eco47III (AfeI equivalent, Thermo Fisher Scientific) and PvuI-HF (New England Biolabs). Parallel to this, pHRW-CRY2Clust was linearised with PvuI-HF (New England Biolabs) and PmeI (New England Biolabs). Fragments of interest from each double digestion were purified from gel, ligated and used to transform competent bacteria to obtain a pHW-CIBN-TRIM_HRW-CRY2Clust double expression vector.

V_HH-mRFP-CRY2Clust_CRY2Clust-TRIM and **mRFP-CRY2Clust-V_HH_CRY2Clust-TRIM:** To generate V_HH-mRFP-CRY2Clust_CRY2Clust-TRIM obtention, a p_{2GT}H-V_HH-RW-CRY2Clust

plasmid was generated by PCR amplification of p_{2GT}H-V_HH-RW-CRY2Clust-TRIM, using primers *pENTR Fw* and *Clust linker Rev* (Table 1), followed by template destruction and competent bacteria transformation. The V_HH-mRFP-CRY2Clust expression cassette was then excised from p_{2GT}H-V_HH-RW-CRY2Clust using AfeI (New England Biolabs) and PvuI (New England Biolabs).

To generate mRFP-CRY2Clust-V_HH_CRY2Clust-TRI, pENTR-CRY2-V_HH (previously described in (**Osswald et al.**, 2019)) was initially amplified by PCR using primers *Cry2Clust Fw* and *Cry2Clust Rev* (Table 1). The template was then destroyed, and the PCR product was used to transform competent bacteria, followed by recombination into a p_{2GT} HRW plasmid to obtain a p_{2GT}HRW-CRY2Clust-V_HH vector. The HRW-CRY2Clust-V_HH expression cassette was then excised from p_{2GT}HRW-CRY2Clust-V_HH using AfeI (New England Biolabs) and PvuI (New England Biolabs).

To obtain the pHW-CRY2Clust-TRIM vector, necessary for both constructs, pENTR-CRY2Clust-TRIM was recombined into a pHW plasmid. pHW-CRY2Clust-TRIM was then linearised with PvuI (New England Biolabs) and PmeI (New England Biolabs). Fragments of interest from all double digestion were purified from gel. Each expression cassette (V_HH-mRFP-Cry2Clust or RFP-Cry2Clust-V_HH) was ligated into the linearised, purified pHW-CRY2Clust-TRIM and used to transform competent bacteria to obtain the pH-V_HH-RW-CRY2Clust_HW-CRY2Clust-TRIM and pHRW-CRY2Clust-V_HH_HW-CRY2Clust-TRIM double expression vectors.

Table 1. Primers used for molecular cloning

Primer name	**Sequence (5' → 3')**
Cry2Clust Fw	GATCCGCCGGACCTGGATAATGTGTACAGTGGGGGAGG
Cry2Clust Rev	CAGGTCCGGCGGATCACGAGCGGCAGCACCGATCAT
pENTR Fw	AAAGGTGGACGCGCTGACCCAGCTTTCTT
Clust linker Rev	ACCACCACCACCACCACCTGAACCA
BBox clon CT Rev	GCGTCCACCTTTTCAAATAGGGACCCTGGT
RINGm	AGCGCGTCCACCTTTTCACTTCTTGGTATTCTG
TRIMh for pENTR Fw	GGTGGTGGTGGTGGTATGGCTTCAGCAGCA
RINGh Rev	AGCGCGTCCACCTTTTCACTCTCTGGCCTCCTG
V_HH for HSP Cterm Fw	AGCTCCGCCACCATGTCTCGAGCCATGGAT
V_HH link RFP Rev	GCTTCCACCTCCAGAGCTGGAGACGGTGAC
V_HH link RFP Fw	TCTGGAGGTGGAAGCGCCTCCTCCGAGGAC
HSP link Rev	CATGGTGGCGGAGCTCCGAATTCACTGCAG
Par6 Fw	GCTGCTCCATTTACAATGTCGAAGAACAAGATAAACAC
Par6 Rev	AGCGCGTCCACCTTTCAAATGCAGCACTCCATC
pENTR Rev	TGTAAATGGAGCAGCCGCGGAGC
TRIM Nlinker Fw	GGTGGTGGTGGTGGTTCTCTGGAAAAGATGTGGG
TRIM for pENTR Rev	AGCGCGTCCACCTTTTCACATCTTTAGTGGACAGAGC
CIB1-MP long linker Rev	ACCACCACCACCACCCGAAGCTTGAGCTCG

S2 cell culture, transfection and induction for live imaging

Drosophila S2-DGRC cells (Drosophila Genomics Resource Center) were cultured at 25°C in Schneider's Insect medium (Sigma-Aldrich, St. Louis, MO, USA) supplemented with 10% fetal bovine serum. Cells were transiently transfected using the Effectene Transfection Reagent (QIAGEN, Hilden, Germany), according to manufacturer's instruction. For single transfections, 1µg of plasmidic DNA was used; for co-transfections, 500ng of each plasmid were used. After transfections, cells were incubated in the dark, but no measure was taken to limit light exposure during cell manipulation prior to induction. Hsp70-promotor controlled constructs were induced by incubation at 37°C for 40 min, at least 5h prior to cell imaging. After induction, cells were kept in the dark and manipulated under a 593nm LED light (Super Bright LEDs, St. Louis, MO, USA), whenever necessary. For live proteasome inhibition assays, culture medium was supplemented with 20µM MG132 (Calbiochem), at least 1h before live imaging.

Live-cell imaging

For imaging, cells were seeded on glass bottom-dishes (MatTek Corporation, Ashland, MA, USA) coated with poly-lysine and filmed in culture medium, at 25°C. Cells were imaged between day 2 and day5 post-transfection. Cells transfected with single plasmids (Figure 5, Figure 6, Figure 8, Supplementary Figure 1) were incubated with CellBrite Green Cytoplasmic Membrane Stain 1x (Biotium, Inc) in 2xSSC buffer (Sigma-Aldrich) for 15 min, immediately before imaging. For live proteasome inhibition assays (Figure 6), the inhibitor supplementation was maintained during imaging, at the same concentration.

All protein depletion live experiments were imaged using a Nikon Ti motorized inverted epifluorescence widefield microscope (Nikon, Japan), equipped with a Lumencor SpectraX light engine and external emission filter wheel, and an Andor iXon888 camera (Andor, UK), with a PL APO LAMBDA 60X OIL/1,4 Oil WD 0,13mm objective, controlled by NIS elements 5.0 (Nikon, Japan) software. Images were acquired along 7 equidistant z-planes, 1.5µm apart. To reduce photobleaching effects detected during the first set of experiments, a new, reduced photobleaching (rp) set of acquisition parameters was used in part of the experiments. Acquisition parameters are summarised in Table 2 and the settings used for each experiment are clearly indicated in all figure legends.

Table 2. Acquisition parameters for live cell imaging

	Channel (absorption/emission)	**Intensity (%)**	**Exposure (ms)**	**Acquisition rate (6 fields/acquisition)**	**Figures/panels**
Initial parameters (ip)	Red (555/602nm)	50	100	Every 60 seconds	Supplementary Figure 1A, Figure 5, Figure 6, Figure 8B-D
	Green (470/525nm)	20	20		
Reduced photobleaching (rp)	Red (555/602nm)	20	20	Every 120 seconds	Supplementary Figure 1B , Figure 8E-G, Figure 10
	Green (470/525nm)	5	20		

Co-clustering experiments (Figure 9) were imaged using an Andor XD Revolution Spinning Disk Confocal system (Andor Technologies, Belfast, United Kingdom) equipped with two solid state lasers (488 nm and 561 nm), an iXonEM+ DU-897 EMCCD camera, and a Yokogawa CSU-22 unit built on an inverted Olympus IX81 microscope (Olympus Corporation, Tokyo, Japan) with a UPLSAPO 100x/NA 1.40 objective, controlled by IQ2 (ANDOR Technology, UK) software.

Echinoid functional assay

Cell culture, transfection and induction

Drosophila S2-DGRC cells (Drosophila Genomics Resource Center) were cultured at 25°C in Schneider's Insect medium (Sigma-Aldrich, St. Louis, MO, USA) supplemented with 10% fetal bovine serum. Cells were transiently transfected using the Effectene Transfection Reagent (QIAGEN, Hilden, Germany), with 500ng of Ed-GFP and 500ng of V_HH-mRFP-CRY2Clust TRIM, according to manufacturer's instruction. Ed-GFP expression was induced with 100µM of $CuSO_4$ 26h before cell fixing. 72h after transfection, cells were exposed to 4 different sets of conditions (Table 3). Heat shocked cells were incubated at 37°C, for 40min, 5h before fixing. Proteasome inhibited cells were supplemented with 20µM of MG132 (Calbiochem), 5h before fixing. Light exposed cells were incubated under a blue (472nm) light (Super Bright LEDs), for 1h, immediately before fixing.

Table 3. Condition setup for Echinoid functional assay

Condition name	Heat Shock	Proteosome inhibition	Light exposure
[–HS –MG +Light]	No	No	Yes
[+HS +MG +Light]	Yes	Yes	Yes
[+HS –MG +Light]	Yes	No	Yes
[+HS –MG –Light]	Yes	No	No

Cell fixing and acquisition

10^5 cells of each condition were centrifuged onto slides for 5min at 1500 rpm (Shandon Cytospin 2, Thermo Fisher Scientific), in the presence of BSA, fixed in 4% paraformaldehyde (Sigma-Aldrich) in PBS buffer for 14min, and then washed with PBS-0.1% Triton X-100 (Sigma-Aldrich) for 8min. Slides were mounted with Vectashield Mounting Medium with DAPI (Vector Laboratories, Burlingame, CA, USA) and imaged with a Zeiss Axio Imager Z1 microscope with Axiocam MR ver3.0 camera (Carl Zeiss, Germany) controlled by Axiovision 4.8 software, using a Plan-Apochromat 40x/1.30 Oil objective. Single plane images were acquired for >20 independent fields for each condition.

Quantification

Protein depletion plots over time

Graphic plots for protein depletion tracking over time (Figure 5C, Figure 6C, Figure 8C & F, Figure 10) are presented in the form of average remaining protein percentage ± standard deviation (STDev) for each timepoint.

To produce these graphs, fluorescence values were measured within regions of interest (ROIs) that included the complete area of each individual cell. Expressing cells in which no visible clustering occurred were not considered. Each ROI's fluorescence was calculated as the average along the 7 z-planes and then normalised for background cellular autofluorescence (3 non-expressing cells were used to obtain the average background fluorescence for each sample).

For each ROI, the remaining protein levels present over time were calculated as the ratio between the ROI's fluorescence for each timepoint and its initial fluorescence. Initial fluorescence was defined as the second timeframe after light-induction to avoid artifactual fluorescence variations caused by the clustering phenomenon onset (see Eq. (1)).

$$Remaining\ protein\ (\%)_{t=x} = \frac{ROI\ fluorescence\ (timepoint\ x)}{Initial\ ROI\ fluorescence\ (timepoint\ 2)} \times 100 \qquad \text{Eq. (1)}$$

Each timepoint was then corrected for photobleaching, by normalisation to 'degradation-negative, clustering-positive' controls using the same acquisition parameters and quantification strategy: mRFP fluorescence was corrected using a mRFP-CRY2Clust expression curve; GFP fluorescence was corrected using the GFP-aPKC expression curve values when co-expressed with pLARIAT_mRFP (see Supplementary Figure 1).

The initial expression plots (Figure 7, Figure 8D & G, Figure 11) depict the initial fluorescence (timepoint 2, as defined above) of the cells included in the expression plots for each condition.

Protein clustering

To obtain the graphs in the co-clustering assays (Figure 9B & D), protein clustering was quantified using the coefficient of variation (CV) as described in (**Osswald et al.**, 2019). Briefly, one ROI over 40μm^2 was created in the cytoplasm of each quantified cell. The CV was calculated for each timepoint as the ratio between the fluorescence intensity standard deviation and the average fluorescence intensity (corrected for background signal) in the same ROI (see Eq. (2)).

$$CV_{t=x} = \frac{ROI\ fluorescence\ STDev\ (timepoint\ x)}{ROI\ fluorescence\ average\ (timepoint\ x)} \qquad \text{Eq. (2)}$$

CV was normalised to its average before cluster formation (CV_i), plotted through time and expressed for each condition as average CV/CV_i + STDev.

Cell adhesion quantification in fixed cells

For the Ed-GFP functional assay quantifications (Figure 12), the GFP transfection (G/T) and GFP+RFP co-transfection efficiency (GR/T) was initially determined. A summary of the calculations is presented in Table 4.

G/T was calculated as the percentage of green-expressing cells out of the total number of cells. Cells that presented green expression outside the expected Ed locations (vesicles, organelle membranes and/or cytoplasmic membrane) were not considered. Cells that

presented the typical Ed-expressing phenotype (visible GFP-expressing line-like adhesions between them) were considered as GFP-expressing cells, even if GFP expression was not detectable anywhere else.

To prevent quantification errors arising from possible basal degradation of RFP-TRIM, the co-transfection efficiency (GR/G) was determined using TRIM21 expressing cells where proteasomal mediated degradation has been blocked. In this condition, co-transfection was considered successful for all non-dividing cells that presented both GFP and RFP-expressing aggregates (regardless of location) and intact-nucleus. Total co-transfection efficiency was assumed to be even for all conditions, where we could not directly measure the transfection efficiency of RFP-TRIM, namely [+HS –MG +Light] and [+HS –MG –Light] for which we inferred the theoretical number of co-transfected cells (Supplementary Table 1)

Table 4. Transfection efficiency calculations in Echinoid functional assay

	Formula (x100)	**Obtention**	
GFP-transfection efficiency (G/T)	GFP-positive cells (G)/ Total number of cells (T)	Quantified	[–HS –MG +Light]
Co-transfection efficiency (GR/G)	GFP&RFP positive cells (GR) /GFP-positive cells	Quantified	[+HS +MG +Light]
Total co-transfection efficiency (GR/T)	GFP&RFP positive cells/ total number of cells	Calculated	(G/T) x (GR/G)

For all conditions, cells were considered to be attached whenever they presented a GFP increased linear-like interface with at least one neighbouring cell, regardless of absolute GFP-intensity or adhesion length. Cells that presented clear mitotic figures were excluded from all quantifications to prevent errors associated with modified detachment during cell division. A total number of non-mitotic cells >1 200 was quantified for each condition. Cell attachment results are presented for each condition in the form of percentage of attached cells out of assumed total number of co-transfected cells.

Statistical analysis and software

Primer design for molecular cloning was optimised using Serial Cloner 2.6.1 by (**SerialBasics**, 2012) and OligoEvaluator online tool by (**Sigma-Aldrich**, 2014). Clust sequence was optimised for Drosophila expression using the online Reverse Translation from Sequence Manipulation Suite (**Stothard**, 2000) combined with a *D. Melanogaster* codon usage table.

Image stacks were assembled, analysed and converted into movies using Fiji/ImageJ software (**Rueden et al.**, 2017; **Schindelin et al.**, 2012). Kymographs (Figure 5B, Figure 6B) were obtained along the indicated dashed lines and pseudo-coloured to match pixel intensity using Fiji's Fire LookUp Table.

Statistical differences between initial expression means (Figure 7, Figure 8D & G, Figure 11) were analysed by application of the unpaired, two-tailed, two sample, heteroscedastic *t*-student test (Welch's *t*-test). To ensure robustness when comparing different sample sizes,

no prior variance calculation was performed before test application. Statistical significance was expressed as "very highly significant" for p-values below 0.001 (***), "highly significant" for p-values between 0.001 and 0.01 (**), or "significant" for p-values between 0.01 and 0.05 (*). Statistical differences between the attached cell proportion in fixed samples (Figure 12) were determined using a standard two-proportion, two-tailed, z-test. Statistical significance was considered with 99% confidence in null hypothesis rejection, corresponding to an absolute critical z-value of 2.5760.

All graphs and statistical analysis were performed using Microsoft Office Excel 2007 (v 12.0.6785.5000) software. All schemes and figures were created and assembled by the author using Microsoft Office Power Point and Publisher 2007, and the online Mind the Graph platform.

▪ Blank page ▪

CHAPTER III

A system for the degradation of light-induced aggregates: development and optimisation

▪ Blank page ▪

Background and aims

Dean Clift et al have recently shown that TRIM21 can recognise free GFP and successfully degrade it upon micro-injection of an anti-GFP Ab in a TRIM21-overexpressing background murine cell line (**Clift et al.**, 2017). Live imaging of this process showed that anti-GFP addition rapidly induces the formation of GFP-Ab aggregates, which the authors attributed to high local concentration of antibody. Interestingly, this observation also raises the possibility that aggregation itself could be serving as the trigger that induces TRIM21-mediated ubiquitination and target clearance. Thus, our group decided to combine light-induced protein aggregation by LARIAT with TRIM21 to determine whether TRIM21 aggregation would be sufficient to induce protein degradation. Preliminary work suggested that this could be indeed the case (Osswald and Morais-de-Sá, unpublished) and so I aimed, during my master thesis, to develop this approach as a tool for temporally controlled protein destabilization, while obviating the need for an external Ab.

In this chapter, we explore the process of optogenetic clustering, coupled to TRIM21 recruitment, to generate a CRY2-based, light-triggered method of inducing TRIM21-mediated degradation. Furthermore, we intended to understand the nature and dynamics of this degradation over time, and identify its limitations, in order to optimise the system's efficiency and temporal resolution. Finally, we explored some alternatives of TRIM21 subdomains that could potentially help overcome the system's limitations in the future.

CRY2Clust-TRIM as a light-based degradation system

We started by testing the ability of a set of different CRY2-based clustering modules to generate light-based degradation-constructs by fusion with TRIM21. In particular, the constructs were compared to determine if they were able to cluster and induce degradation in a time-efficient manner. All constructs were tagged with mRFP (Figure 5A) and used to transfect *Drosophila* S2 cells, where the TRIM21 ubiquitination system is normally absent. Applying a protocol similar to that of LARIAT, the system was triggered by application of a 470nm, blue light stimulus compatible with the activation of CRY2 clustering, and mRFP fluorescence was tracked through live-imaging.

Given that CRY2 and TRIM21 both have the intrinsic ability to homo-oligomerise (**Foss et al.**, 2015; **S. Lee et al.**, 2014), we started by simply fusing TRIM C-terminally of an mRFP tagged CRY2 domain. The resulting mRFP-CRY2-TRIM construct underwent visible clustering and subsequent degradation within few minutes after light triggering (Figure 5A & B, Movie S2) and the initial pool of mRFP was nearly halved in less than an hour (Figure 5C). Because leftover non-aggregated protein was still visible in the cytoplasm of most cells, we hypothesised that clustering efficiency could be one of the limiting factors in the system. In an attempt to overcome this limitation, we fused the Clust peptide, which was recently described as having the ability to improve aggregation (**Park et al.**, 2017), to the CRY2 domain. The resulting mRFP-CRY2Clust underwent efficient and sustained light triggered clustering (Figure 5A & B, Movie S1), unlike mRFP-CRY2 without Clust (**Osswald et al.**, 2019).

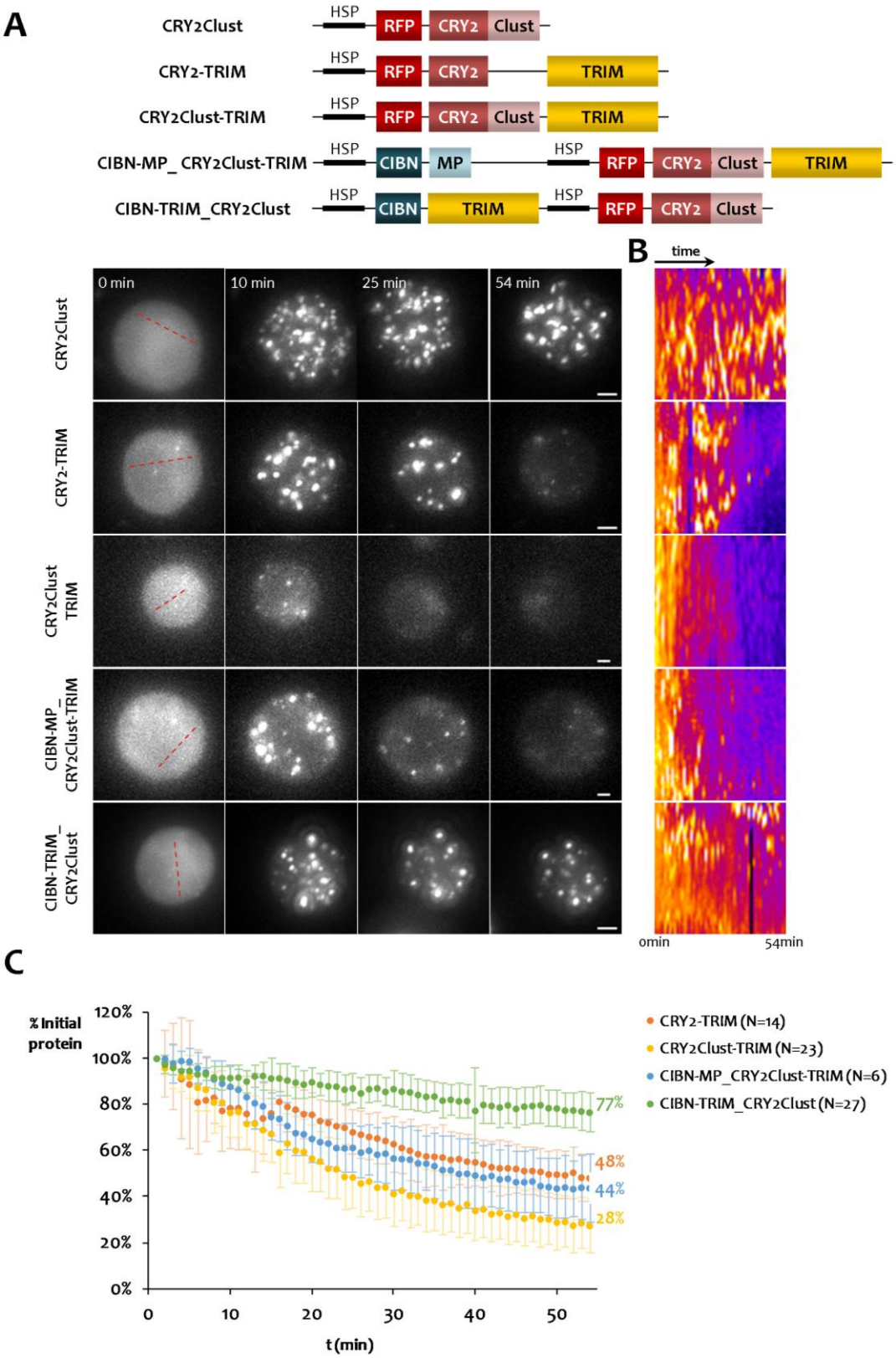

Figure 5. mRFP-CRY2Clust-TRIM is the most effective light induced self-destabilisation module

mRFP-CRY2Clust, mRFP-CRY2-TRIM, mRFP-CRY2Clust-TRIM, CIBN-MP_mRFP-CRY2Clust-TRIM, and CIBN-TRIM_mRFP-CRY2Clust were compared by live imaging of mRFP after blue (470nm)-light induction of clustering at min 0. (A) Schematic representation, abbreviated names and representative stills, and (**B**) kymographs for mRFP expression along the dashed lines are shown for all constructs. (**C**) Intensity profiles over time of the percentage of remaining protein are shown for all TRIM-containing constructs. Final percentages correspond to min 54.

[Initial parameters of acquisition were used. Scale bar = 2.5µm. All plot timepoints are normalised for CRY2Clust]

mRFP-CRY2Clust efficient aggregation without anticipated degradation led us to use it as a negative control for degradation, which is particularly useful to remove the contribution of photobleaching in signal decay of the proteins fused with TRIM21. Consistent with the increased aggregation efficiency of CRY2Clust, mRFP-CRY2Clust-TRIM underwent rapid aggregation (Figure 5A & B, Movie S3) and its degradation efficiency was notably increased by Clust, with over 70% of the initial pool of protein depleted within one hour (Figure 5C).

These results highlighted the importance of the clustering process to determine the overall efficiency of the degradation system. In line with this, we attempted to further improve aggregation by combining the CRY2Clust-TRIM21 module with an oligomeric form of the CRY2-interacting domain CIBN (**S. Lee et al.**, 2014), which was expressed under the control of a separate promoter within the same plasmid. The resulting CIBN-MP_mRFP-CRY2Clust-TRIM presented rapid light-induced aggregation of the mRFP tagged module (Movie S4, Figure 5A & B). However, this construct was less efficient in degradation, with the aggregates persisting for a longer amount of time in the cytoplasm. To test an alternative mechanism for TRIM recruitment to the aggregates, we attempted to fuse TRIM21 to CIBN in a separate module from mRFP-CRY2Clust. CIBN-TRIM_mRFP-CRY2Clust was able to aggregate efficiently, but aggregate clearance was very poor (Figure 5A & B, Movie S5), and protein degradation was the least effective out of all constructs (Figure 5C). Thus, even though clustering is a key factor, the position of TRIM21 within the clustering module might be equally important to achieve effective clearance, and a balance must be struck between the addition of oligomerisation units that improve clustering and their potentially negative effects on TRIM21's activity. In this sense, out of all the constructs tested, mRFP-CRY2Clust-TRIM stood out as the most promising clustering module to use in the subsequent development of our light-induced degradation tool.

Activity of the CRY2Clust-TRIM21 requires proteasomal degradation

To confirm that the fluorescence decay seen in the previous experiment was due to proteasomal degradation via the UPS system, mRFP-CRY2Clust-TRIM was tested in the presence of a proteasome inhibitor, MG132. Upon inhibitor supplementation, the system still formed light-induced clusters (Figure 6A, Movie S9), but degradation was almost entirely rescued to the levels of the mRFP-CRY2Clust control (Figure 6B & C). These results are consistent with previous reports on TRIM21's endogenous activity (**Mallery et al.**, 2010), as well as TRIM21's behaviour in the Trim-Away system, which was also sensitive to MG132 inhibition (**Clift et al.**, 2017).

Therefore, our results validate the involvement of the UPS as a major pathway in TRIM21-mediated degradation upon light-induced clustering.

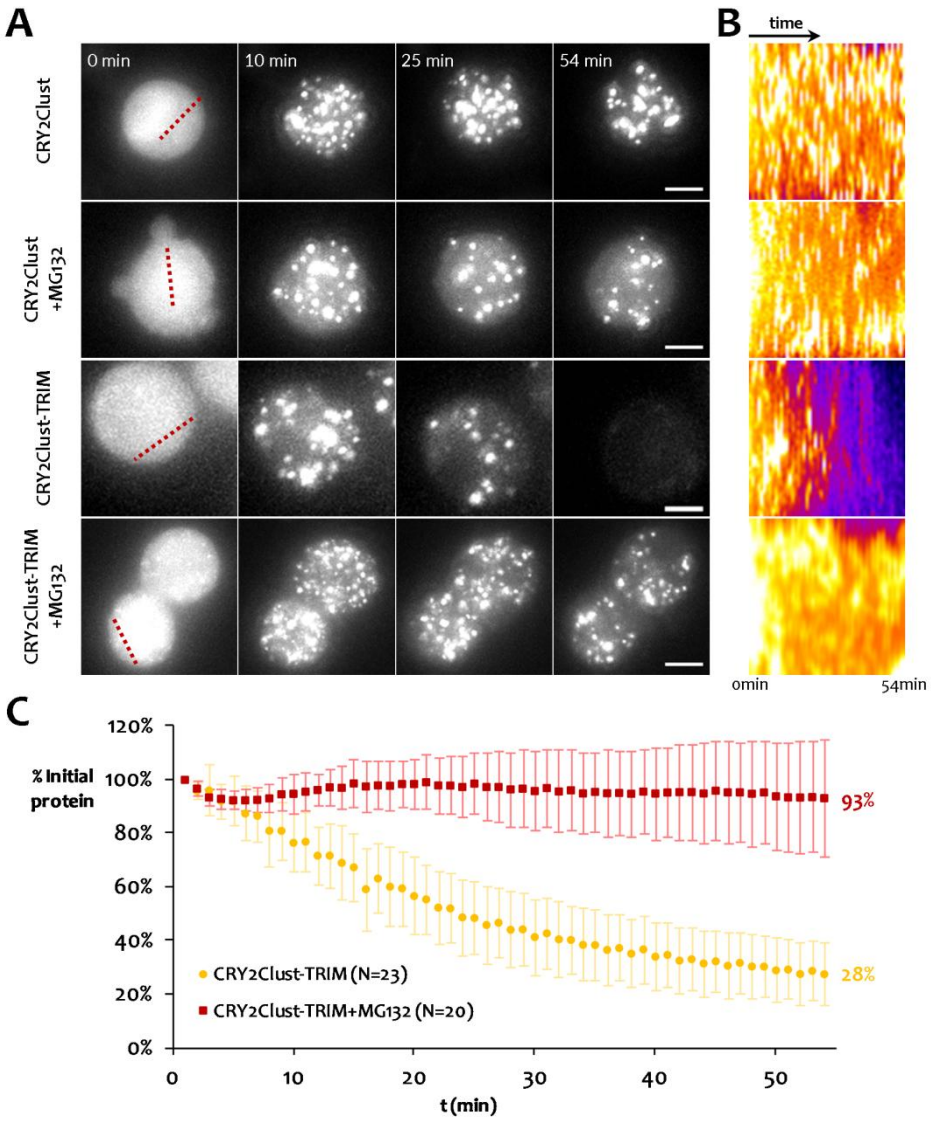

Figure 6. Decrease of mRFP-Cry2Clust-TRIM levels upon light-induced clustering is proteasome dependant

mRFP-CRY2Clust and mRFP-CRY2ClustTRIM were analysed by live imaging of mRFP after blue (470nm)-light induction of clustering at min 0, with or without the addition of proteasome inhibitor MG132. (**A**) Representative stills, and (**B**) kymographs of mRFP expression along the dashed lines are shown for all conditions. (**C**) Intensity profiles over time of the percentage of remaining protein are shown. Final percentages correspond to min 54.

[Scale bar = 5µm. Timepoints for the proteasome inhibited and the non-proteasome inhibited conditions are normalised for CRY2Clust, with or without MG132, respectively (see Supplementary Figure 1).]

Basal degradation before light-exposure as a possible system limitation

Even though TRIM21's endogenous mechanisms of action in the immune response are still very poorly understood, it is known that TRIM21, similarly to other E3 ligases, is prone to auto-ubiquitination (**Espinosa et al.**, 2006). When observing the levels of protein at the onset of live-imaging experiments, we noticed a tendency amongst efficient-degrading constructs to express lower amounts of protein than those whose degradation was less efficient. This led us to inquire whether these constructs could be undergoing degradation, due to TRIM21's auto-ubiquitination. To illustrate this, initial protein expression levels prior to blue light exposure were plotted in Figure 7 for all constructs.

mRFP-CRY2-TRIM, mRFP-CRY2Clust-TRIM and CIBN-TRIM_mRFP-CRY2Clust-TRIM constructs all presented initial expression levels significantly lower than that of the non-degradative control, mRFP-CRY2Clust. This is to say that the three constructs with the highest degradation efficiencies (Figure 5C) undergo basal degradation between the moment when construct expression is induced by heat shock and the onset of imaging (≈5h). Accordingly, mRFP-CRY2Clust-TRIM expressing cells showed higher expressing levels when MG132 was added at least 1h before imaging.

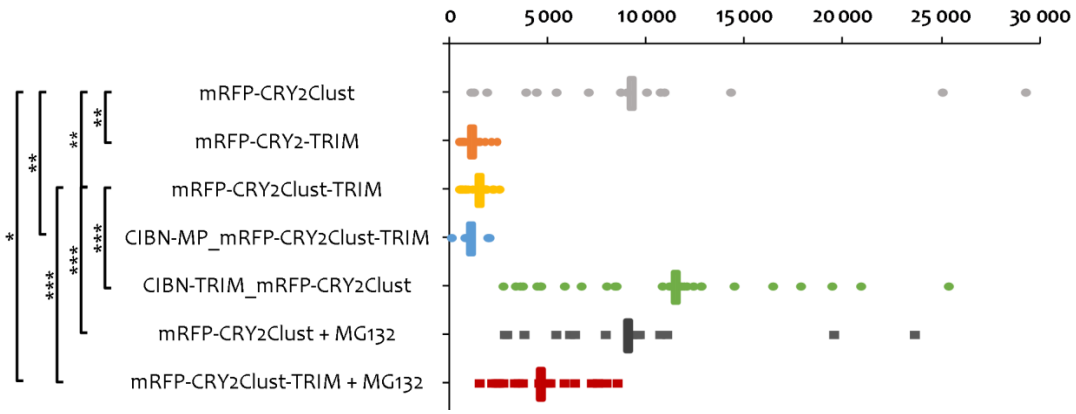

Figure 7. Basal destabilization of mRFP is observed when mRFP is fused with TRIM21 within the same protein

Initial mRFP expression of mRFP-CRY2Clust (with or without MG132), mRFP-CRY2-TRIM, mRFP-CRY2Clust-TRIM (with or without MG132), CIBN-MP_mRFP-CRY2Clust-TRIM, CIBN-TRIM_ mRFP-CRY2Clust constructs before exposure to 470nm laser is shown in arbitrary units. The three constructs where TRIM21 and mRFP were combined in the same protein presented lower initial mRFP expression compared to the control. Low expression levels were partially rescued, in the case of mRFP-Cry2Clust-TRIM, by proteasome inhibition with MG132.

[Each point represents an individual cell. Vertical dashes represent the average for each condition. *0.01<p<0.05, **0.001<p<0.01, ***p<0.001, unpaired, two tailed, two-sample heteroscedastic t-student test.]

Given that this system aims at the co-degradation of target proteins specifically after the light input, basal degradation would pose a threat to the functionality of the system, as it could lead to premature destabilisation of the protein of interest. This would therefore decrease the temporal resolution of optogenetic control. Interestingly, CIBN-TRIM_mRFP-CRY2Clust showed no difference in initial mRFP expression when compared to the control (Figure 7). However, in this construct, TRIM21 is under a separate protein than that of mRFP, and we cannot conclude whether the CIBN-TRIM untagged module was suffering basal degradation by auto-ubiquitination or not. In contrast, for all constructs that presented lower initial expression levels, the mRFP protein whose fluorescence we used as readout was fused in tandem with TRIM21 and also with CRY2, which may or may not be affecting TRIM21's ability to protect itself from degradation. These results served as a note of caution and the aspect of basal degradation was considered in the subsequent experiments.

Finding a minimal functional subunit for TRIM21-mediated degradation

TRIM21 is a multi-domain protein constituted by an N-terminal RBCC motif and a C-terminal PRYSPRY domain (Figure 8A, (**Oke et al.**, 2012)), that is responsible for recognition and binding to the Fc portion of antibodies (**Keeble et al.**, 2008).

Given that our system does not rely on antibodies for TRIM21 recruitment, we hypothesised that a construct lacking the PRYSPRY domain would still be usable for light-induced degradation. Moreover, fusion to CRY2Clust should be enough to engage TRIM21 activity upon aggregation, even in the absence of the CC domain, which is normally involved in the oligomerisation of RBCC-containing proteins (**Mallery et al.**, 2010). We therefore used live imaging to compare mRFP-CRY2Clust-TRIM to a version of the construct containing only the RING and B-Box (aa 1-123) domains, which are necessary for E3 Ub-ligase activity and its regulation, respectively (**Dickson et al.**, 2018; **Espinosa et al.**, 2006; **Wallenhammar et al.**, 2017). mRFP-CRY2Clust-RING+BBox was able to trigger degradation, albeit almost 20% less effectively than the full TRIM21 version (Figure 8B & C, Movie S11). The persistence of a significant amount of protein that remained unclustered in the cytoplasm (Figure 8B) suggests that maybe the CC domain could contribute towards the aggregation of the full TRIM21 module, improving overall efficiency. Alternatively, C-terminal depletion could have indirectly affected E3 ligase activity. Wallenhammar et al. structural observation that the B-Box can simultaneously interact with RING and the CC domain led them to propose that the B-Box could act as a plastic inter-domain joint that regulates the overall modular arrangement of the protein (**Wallenhammar et al.**, 2017). Our CC domain depleted construct could therefore be locking the RING+B-Box in a sterically auto-inhibited (or at least less active) state. This possibility would be in line with the results we obtained for the initial protein expressions levels (Figure 8D), as mRFP-CRY2Clust-RING+BBox presents significantly higher levels of initial protein when compared to the full TRIM21 version, with an average initial expression similar to that of the control. This suggests that no basal degradation is occurring and that the B-Box might be acting as a strong RING repressor in the absence of the C-terminal portion of the protein.

Therefore, an mRFP-CRY2Clust-RINGm construct including only the RING region of mouse TRIM21 (aa 1-76) was generated to determine whether the B-Box was indeed negatively affecting RING E3 ligase activity. Upon light induction, mRFP-CRY2Clust-RINGm formed very small clusters, that cleared away very quickly (Figure 8E, Movie S13). Overall, mRFP-CRY2Clust-RINGm was only slightly more efficient than mRFP-CRY2Clust-RING+BBox at degradation (Figure 8F). However, mRFP-Cry2Clust-RINGm seems to be more prone to basal degradation than the CRY2Clust version with the full TRIM construct (Figure 8G), whereas cells express higher initial levels of mRFP-Cry2Clust-RINGBbox (Figure 8C). Thus, the presence of the B-Box without the CC domain seems sufficient to impair basal degradation. Nevertheless, whereas the B-Box does not fully repress RING activity upon clustering, the absence of the C-terminal portion of the protein may be impairing overall effectiveness of light-induced degradation.

These findings could be important to fine tune the final system aiming at a balance between minimal basal degradation and maximum degradation efficiency by exploring other TRIM21 sub-domain combinations.

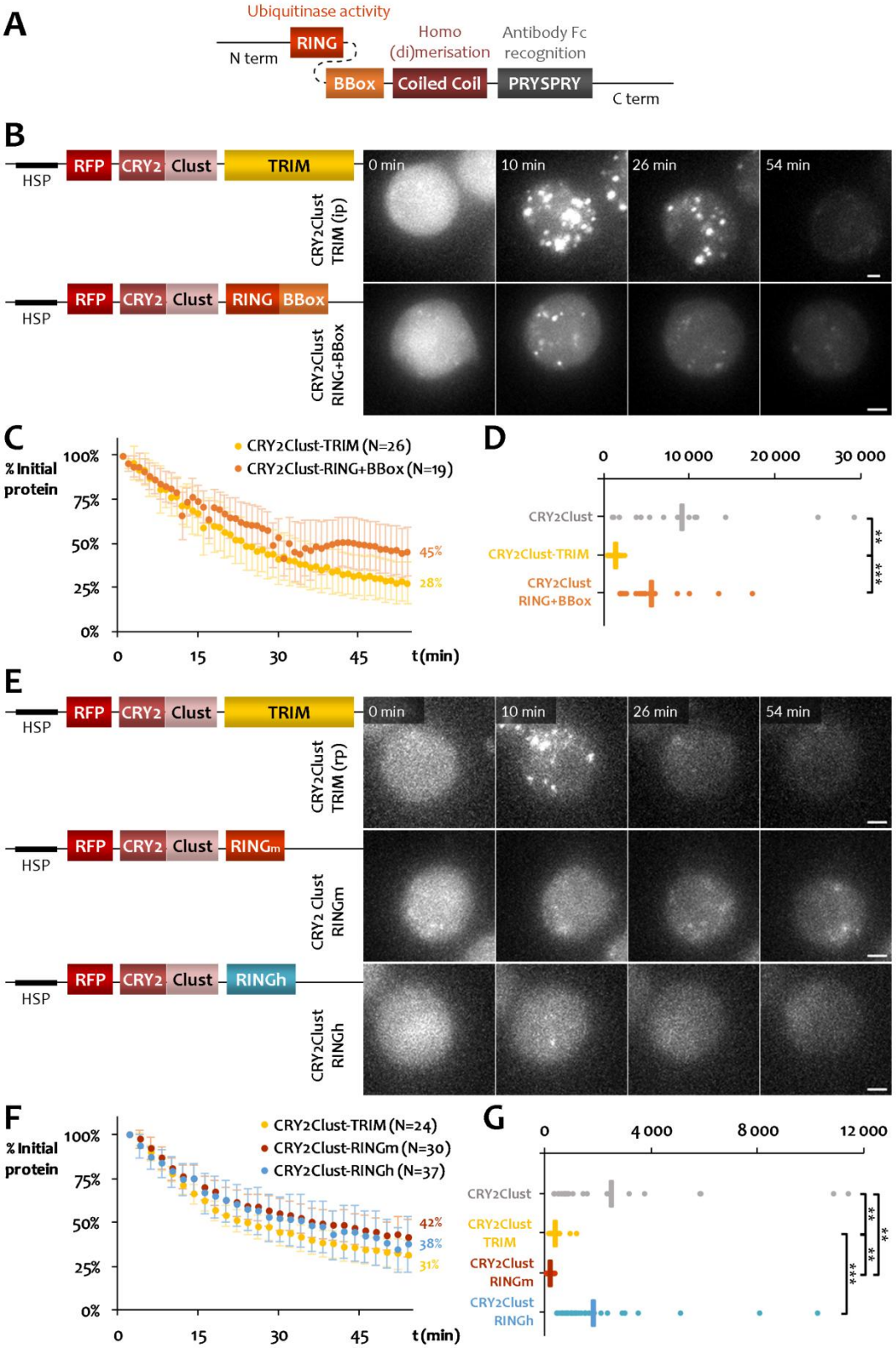

Figure 8. RING and RING+BBox constructs induce degradation but are less efficient than full length TRIM.

(A) Schematic representation of TRIM21 subdomains. mRFP-CRY2Clust-TRIM, mRFP-CRY2Clust-RING+BBox, mRFP-CRY2Clust-RINGm, and mRFP-CRY2Clust-RINGh expressing S2 cells were analysed through mRFP live imaging. Clustering was triggered at min 0 (470nm laser). (**B & E**) Constructs and representative stills are shown. Final percentages correspond to min 54. [Scale bar = 2.5µm. Initial (ip) and reduced photobleaching (rp) acquisition parameters were used to in B and E, respectively, and timepoints are normalised for mRFP-CRY2Clust accordingly.]. (C & F) Intensity profiles over time of the percentage of remaining protein are shown. (**D & H**) mRFP expression before exposure to 470nm laser is shown in arbitrary units for the indicated proteins. [Each point represents an individual cell. Vertical dashes represent the average for each condition. **0.001<p<0.01, ***p<0.001, unpaired, two tailed, two-sample heteroscedastic t-student test.]

TRIM21 is a structurally conserved protein amongst mammals, and there is considerable homology between human and mouse TRIM21 (**Keeble et al.**, 2008). However, having first been identified in human auto-immune patients, human TRIM21 is, understandably, much better characterised than mouse TRIM21. Contrary to human TRIM21, whose RING and BBox domains have been resolved and are relatively well characterised (**Anandapadamanaban et al.**, 2019; **James et al.**, 2007; **Wallenhammar et al.**, 2017), not many studies have focused on the RBCC motif in *Mus musculus*. We therefore decided to test a version of human RING (aa 1-85) and compare its efficiency to our mouse TRIM21-derived constructs.

Similarly to mouse RING (denoted RINGm), the human RING (denoted RINGh) module formed small clusters that rapidly cleared from the cytoplasm upon light triggering (Figure 8E, Movie S14). mRFP-CRY2Clust-RINGh overall degradation efficiency was slightly better than that of RINGm, coming close to the results obtained with the full mouse TRIM construct (Figure 8F). One interesting aspect of the RINGh construct was its ability to achieve higher initial expression levels, which may result from a lower tendency for basal degradation. In fact, mRFP-CRY2Clust-RINGh initial protein levels were not reduced in comparison to mRFP-CRY2Clust, and were significantly higher than those of mRFP-CRY2Clust-TRIM and mRFP-CRY2Clust-RINGm (Figure 8G). This suggests that, at least in *Drosophila* cells, human TRIM21 may be less prone to basal auto-ubiquitination prior to light induced clustering.

CHAPTER IV

System application to the targeted recruitment and degradation of proteins of interest

▪ Blank page ▪

Parts of this chapter have been published as:

Osswald, M.; Santos, A.F.; Morais-de-Sá, E.

Light-Induced Protein Clustering for Optogenetic Interference and Protein Interaction Analysis in *Drosophila* S2 Cells. *Biomolecules* **2019**, 9, 61.

doi:10.3390/biom9020061

Author contribution to experimental work in this chapter:

Co-clustering experiments were done in collaboration with M. Osswald. All other experiments and data analysis were performed by A.F. Santos.

Background and aims

In the development of a tool for targeted POI degradation, and regardless of the kinetics and potential for degradation that the system might present, the ability to specifically target and recruit the POI is absolutely key. Herein, we will be making use of a V_HH nanobody to recruit POIs

The V_HH nanobody: a small unit with a big role

The V_HH nanobody has the potential to recognise and recruit POIs that bear a common GFP fusion tag. Nanobodies are derived from *Camalidae* atypical immunoglobulins, and they constitute their smallest antigen binding fragment (**Rothbauer et al.**, 2006). Rothbauer et al. initially isolated an anti-GFP nanobody, V_HH(GFP) (herein termed simply V_HH) from lymphocytes of a GFP-immunised alpaca, and characterised its distribution, access to cellular compartments and antigen binding potential. The fact that GFP-fusion transgenes including GFP in the *Drosophila* genome are widely available for imaging obviates the need for further genetic alterations in the POI. This led the authors of the LARIAT system to choose this nanobody to improve the versatility of the tool and recruit any GFP-tagged protein to their light induced clusters (**S. Lee et al.**, 2014).

In this chapter, the V_HH nanobody will be used to enable the recruitment of POIs to light-induced clusters. Firstly, we explored this tool to detect protein-protein interactions, using as a proof of concept the established interaction between the cell polarity regulators aPKC and Par6. Secondly, we used it to test if recruitment of GFP-tagged proteins to light-induced TRIM21 aggregates would result in subsequent co-degradation of the POI. Finally, we will discuss the results of a functional assay, where we applied this system to interfere with cell-cell adhesion, to test if it could elicit a visible loss-of-function phenotype.

Optogenetic clustering for protein recruitment and detections of protein interactions

To test the ability of V_HH to recruit GFP-tagged proteins to light-induced clusters and probe their interaction with other proteins within the cellular context, we used two tagged proteins involved in polarity regulation during asymmetric cell division, epithelial morphogenesis, and directed cell migration: **Par**titioning defective protein 6 (Par6) and **a**typical **P**rotein **K**inase **C** (aPKC) (**Suzuki et al.**, 2002). aPKC and Par6 are part of a trimeric

complex that localises in tight junctions in polarised cells, and they heterodimerise by interaction between their respective Phox and Bem1 (PB1) domains, located at the N-terminal of each protein (**Noda et al.**, 2003). S2 cells were co-transfected with a GFP-tagged aPKC construct, an mRFP tagged Par6 construct (Figure 9B), and a pLARIAT encoding for the full LARIAT module, including the V_HH unit (Figure 9A). The aPKC/Par6 complex was disperse in the cytoplasm of *Drosophila* S2 cells before stimulation. Upon CRY2 activation with blue light, however, both proteins underwent clustering in under 1 minute (Figure 9C). Clusters were mobile and grew in size over time (Movie S15). In order to quantify co-clustering through time, the coefficient of fluorescence variation (CV), which is a measure of the STDev intensity in the cytoplasm, was plotted. Importantly, CV does not represent an absolute measure of clustering levels, but rather an appropriate representation of the dynamics of cluster formation, because aggregation increases the amplitude of

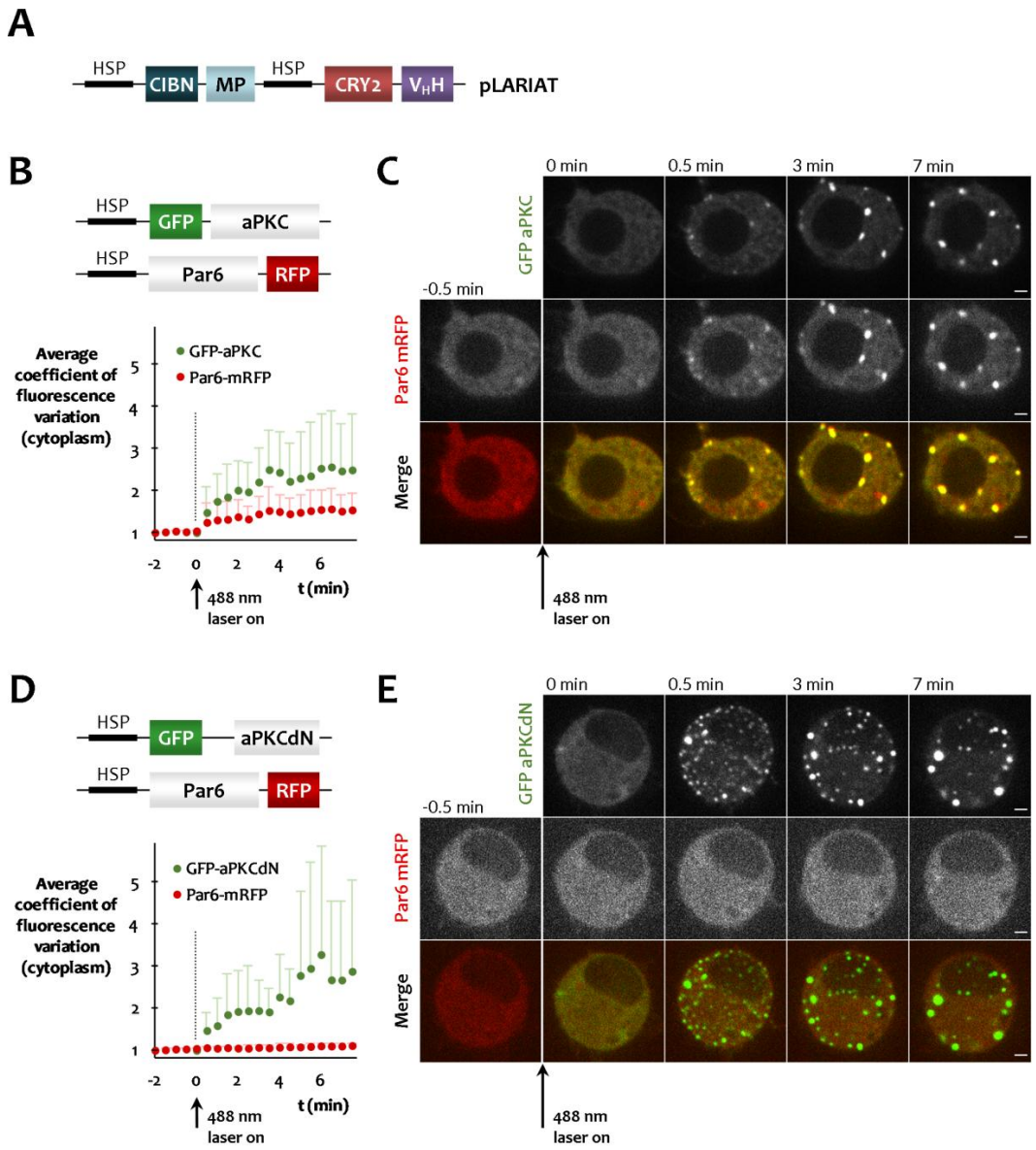

Figure 9. V_HH recruits GFP-tagged aPKC and its binding partner Par6 to light-induced clusters in S2 cells

S2 cells were live imaged after co-transfection of Par6-mRFP together with (**A**) V_HH containing construct pLARIAT, and either (**B** & **C**) GFP-aPKC (n=18), or (**D** & **E**) GFP-aPKCdN (n=16). Clustering was triggered at min 0 (488nm laser). (**B** & **D**) Clustering is represented by the coefficient of variation of cytoplasm fluorescence. Graphs display mean + STDev. (**C** & **E**) Representative stills are shown. [Scale bar = 2.5µm.]

fluorescence levels within a cell due to local accumulation in the clusters with concomitant fluorescence decay in the cytoplasm. Our results show that GFP-aPKC and Par6-mRFP cluster simultaneously, which translates into a similar curve shape between the two protein plots (Figure 9B). Moreover, Par6-mRFP and GFP-aPKC co-localize in the clusters (Figure 9C) as would be anticipated by their ability to form a protein complex (**Suzuki et al.**, 2002). In contrast, when repeating the same experiment using GFP-aPKCdN, which lacks the N-terminal PB1 domain region required for interaction, Par6-mRFP failed to localise to the clusters (Figure 9E, Movie S16), resulting in a "flat" curve in the CV plot due to the maintenance of fluorescence homogeneity over time (Figure 9D).

This assay highlighted the potential of light-induced clustering to evaluate protein interactions, which paves way for its application in live protein interaction studies and structure-function analysis in temporally restricted processes. Moreover, it validated the use of V_HH fusions to CRY2 as an approach to recruit GFP-tagged proteins together with their binding partners, which we subsequently explored in the context of TRIM21-mediated degradation.

Optogenetic clustering to induce targeted protein degradation

We engineered V_HH into constructs containing the CRY2Clust-TRIM module to test if proteins could be successfully recruited to light-induced clusters and subsequently targeted for degradation. We generated a construct where V_HH was fused in the TRIM21 module and we also attempted to prevent premature degradation of the POI before light exposure by the generation of constructs that included the Cry2Clust-TRIM21 degradation module separated from the V_HH recruitment module. Light-induced cluster formation occurred for all constructs, with positive co-localisation of mRFP and GFP tags, suggesting that V_HH is able to recruit GFP-aPKC to the clusters in all conditions (Figure 10, right panels, Movie S17-S19). However, both double promoter constructs were much less efficient than V_HH-mRFP-CRY2Clust-TRIM, regardless of V_HH position in the construct (Figure 10B & C, left panels), with only about 30% of the POI is degraded within 1 hour. In contrast, the kinetics of V_HH-mRFP-CRY2Clust-TRIM was much faster, and led to the depletion of over 70% of the initial aPKC pool within 1 hour (Figure 10A, left panels). Interestingly, and for all constructs, the GFP-tagged POI was depleted faster than the corresponding mRFP-tagged recognition/clustering module, which is consistent with results reported for the Trim-away system (**Clift et al.**, 2017). Additionally, the degradation kinetics and the ultimate stabilisation of levels at around 30% of the initial levels of the POI for V_HH-mRFP-Cry2Clust-TRIM are similar to the self-degradation profile of mRFP-Cry2Clust-TRIM, which is the most efficient construct tested in CHAPTER III (Figure 8F & Figure 10A, left panel). Notably, the authors of Trim-away reported similarly shaped kinetic profiles for membrane-anchored GFP, and chromatin-bound GFP, with around 30% of the initial POI levels left 60 min after Ab addition (**Clift et al.**, 2017). It is possible that this corresponds to a minimal threshold, below which the low concentration of the clustering or degradation units will no longer trigger degradation.

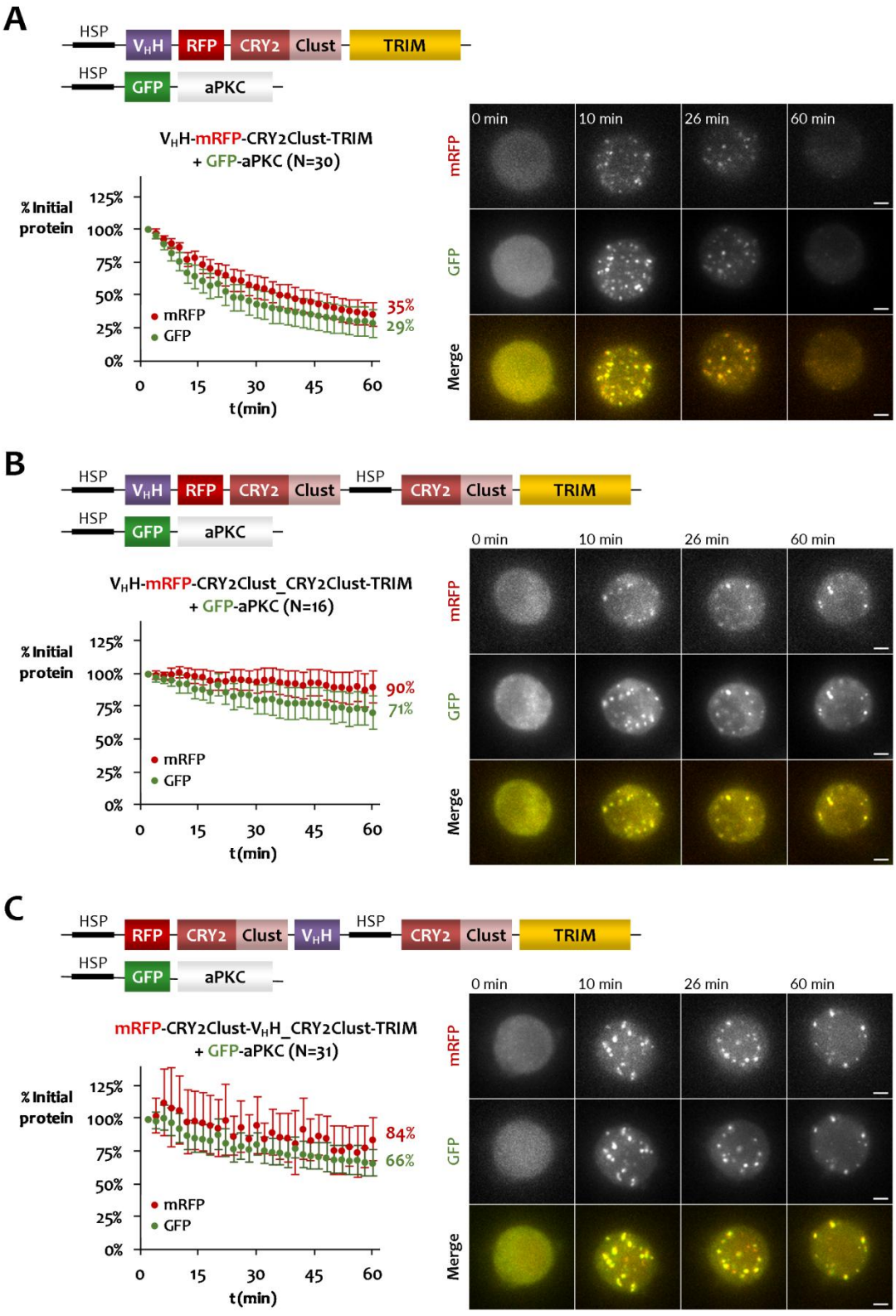

Figure 10. V_HH-mRFP-CRY2Clust-TRIM efficiently recruits GFP-aPKC to light induced aggregates for TRIM21-mediated degradation

S2 cells co-expressing GFP-aPKC and either (**A**) V_HH-mRFP-CRY2Clust-TRIM, (**B**) V_HH-mRFP-CRY2Clust_CRY2Clust-TRIM or (**C**) mRFP-CRY2Clust-V_HH _CRY2Clust-TRIM were analysed through live imaging. Clustering was triggered at min 0 (470nm laser). Intensity profiles show the percentage of remaining protein over time on the left whereas representative stills are shown on the right.

[Reduced photobleaching parameters of acquisition were used. All mRFP and GFP timepoints are corrected for photobleaching by normalisation against mRFP-CRY2Clust and GFP-aPKC co-expressed with LARIAT, respectively (see Supplementary Figure 1). Scale bar = 2.5µm]

In fact, this would be consistent with the inverted exponential-like shape of the depletion curves. Clift and colleagues performed quantification of antibody and TRIM21 levels compared to POI using Trim-away, and proposed that an excess of TRIM21 was indeed required to facilitate degradation and avoid system limitation (**Clift et al.**, 2017). With this in mind, the basal degradation that we described in the previous chapter is particularly relevant. TRIM21 auto-ubiquitination without light input could be lowering the levels of the Cry2Clust-TRIM module so that it would become a limiting factor to enable degradation of the POI. We thus analysed initial mRFP expression levels for all V_HH containing constructs prior to light-induced activation (Figure 11B). All of the V_HH constructs presented significantly lowered initial expression, including the V_HH-mRFP-CRY2Clust-TRIM, which means that basal destabilisation of the TRIM21 unit does not account *per se* for the different degradation efficiencies presented by the constructs.

Basal degradation of the system's modules raises the concern that the POI could also be destabilised prior to light activation, with a consequent loss of temporal control over the system, as discussed previously in CHAPTER III. To assess this possibility, the GFP-aPKC

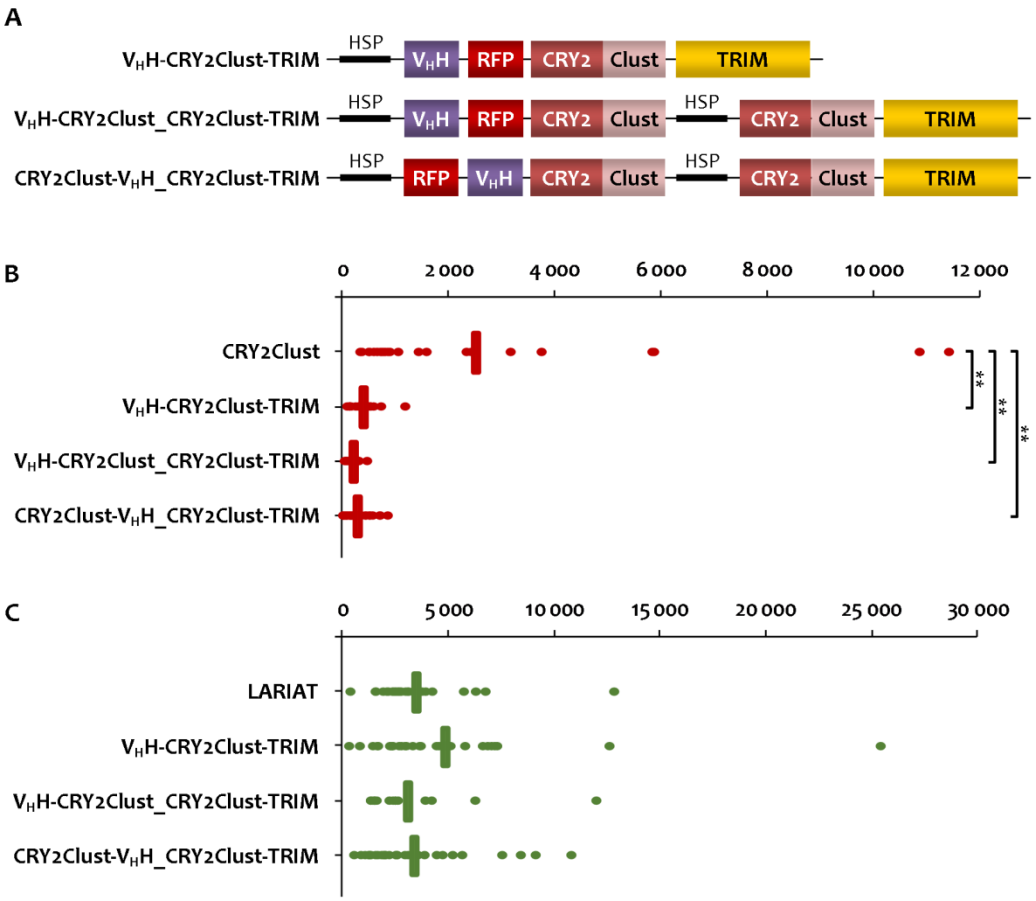

Figure 11. Basal degradation of the TRIM21 component does not cause basal degradation of the GFP-tagged POI

(**A**) V_HH-mRFP-CRY2Clust-TRIM, V_HH-mRFP-CRY2Clust_CRY2Clust-TRIM, and mRFP-CRY2Clust-V_HH_CRY2Clust-TRIM construct schematics and name abbreviations, and initial expression before exposure to 470nm laser of (**B**) mRFP, and of (**C**) co-transfected GFP-aPKC, are shown in arbitrary units.

[mRFP-CRY2Clust initial expression is presented in (**B**) as a negative control for mRFP basal degradation. GFP-aPKC initial expression when co-transfected with LARIAT is presented in (**C**) as a negative control for GFP basal degradation. Each point represents an individual cell. Vertical dashes represent the average for each condition. **0.001<p<0.01, unpaired, two tailed, two-sample heteroscedastic t-student test.]

initial expression levels were also plotted and compared (Figure 11C). GFP-aPKC initial expression when co-expressed with LARIAT was used as a negative control for basal degradation, given that LARIAT does not possess a TRIM21 domain of any kind. Importantly, no significant differences were found between any of the conditions. Thus, the POI anchored to the TRIM21 module via the V_HH nanobody appears to be protected from TRIM21's mechanism of auto-ubiquitination in the absence of induced clustering.

Overall, although basal degradation in our system may still pose a problem to deplete very abundant POIs by limiting the amount of Cry2Clust-TRIM21 available, these results lower the concern associated with premature destabilisation of the POI prior to the activation of light-induced clustering. V_HH-mRFP-Cry2Clust-TRIM has the most appropriate stoichiometry of the degradation and clustering components, showing good potential to elicit efficient degradation of a POI, without compromising its levels prior to system activation.

Application of optogenetic induced clustering and degradation to interfere with proteins that regulate cell-cell adhesion

We sought to validate our system using a protein with interest in the context of cellular adhesion. Membrane-bound cellular adhesion proteins pose a particular challenge for targeted depletion, because they are often part of larger complexes, and can establish very strong interactions with the cytoskeleton and/or adjacent cells. Their study during cell division, which is the main research focus in our group, asks for refined temporal control over depletion to achieve POI elimination within a time window compatible with division timing.

We chose to test the effects of our system upon the induction of S2 cell adhesion using Echinoid (Ed), a transmembranar protein with an intracellular C-terminal domain that binds cytoskeletal actin filaments. Together with DE-Cadherin, Ed mediates cell-cell adhesion at adherens junctions in epithelial polarised cells (**Wei et al.**, 2005). S2 cells do not express endogenous functional Ed. However, when transfected with exogenous Ed, S2 establish cell-cell contacts through intercellular interactions by this homophilic adhesion molecule. Ed can also be found in endocytic vesicles in the cytoplasm (**Rawlins et al.**, 2003).

We co-transfected S2 cells with a GFP-tagged Ed construct expressed under the metallotonein Cu^{2+} promoter (Cu^{2+} inducible) and the V_HH-mRFP-CRY2Clust-TRIM construct, which is under a heat shock promoter (Figure 12A). Cells not exposed to heat shock expressed Ed at the expected localisation (Figure 12C) and showed 84% of Ed-GFP expressing cell attached (Figure 12B). Moreover, groups of more than one attached cells were frequent (up to 11 cells attached between them) (not shown).

We then attempted to elicit a loss of adhesion phenotype by heat shock induction of the V_HH-mRFP-CRY2Clust-TRIM followed by activation by blue (488nm) light. After 1 hour of light exposure, the percentage of adhesions was significantly lower than non-induced cells, with only 45% showing attachment. When present, adhesions often showed lower Ed-GFP expression and smaller cell-cell interfaces (Figure 12D). mRFP expression co-localised with

Ed-GFP at cell-cell adhesions (Figure 12D, arrows), suggesting that the recruitment of the TRIM21 module to Ed-mediated adhesion sites could play a role in adhesion destabilisation.

Even though V_HH-mRFP-CRY2Clust-TRIM co-expression with GFP-aPKC did not result in POI basal degradation, we hypothesised that TRIM could be recognising high local concentrations of Ed-GFP at cell-cell adhesions and vesicles as aggregates, thereby

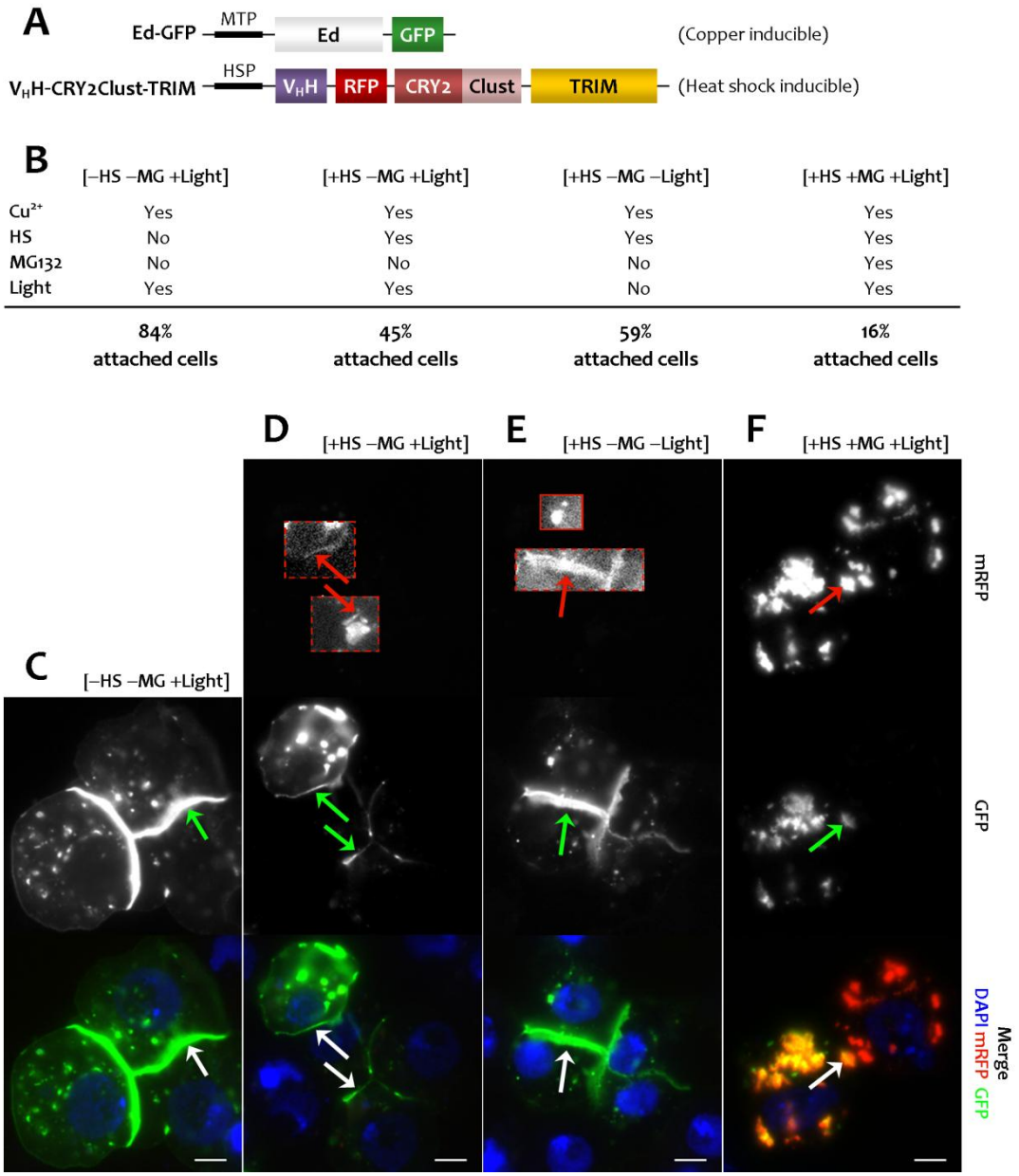

Figure 12. V_HH-mRFP-CRY2Clust-TRIM transfection causes loss of GFP-tagged-Ed mediated adhesions in S2 cells

S2 cells were co-transfected with (**A**) Ed-GFP and V_HH-mRFP-CRY2Clust-TRIM [MTP = Metallothionein promoter; HSP = Hsp70 promoter] and subsequently submitted to (**B**) the indicated conditions of Cu2+ induction, heat shock (HS), proteasome inhibition (MG132) and exposure to blue (488nm) light. The percentage of attached cells out of the total number of GFP-transfected cells is shown for [-HS –MG +Light]. The percentage of attached cells out of the total number of co-transfected GFP&RFP positive cells is shown for all other conditions. Differences between all four conditions are statistically significant (99% confidence, two-proportion, two-tailed z-test). [Results of transfection efficiencies are shown in Supplementary Table 1.]. (**C-F**) Fixed cells images showing adhesions for each indicated condition are shown. Arrows indicate cell-cell adhesions. Insets show mRFP expression with increased white-balanced parameters to allow visualisation. Dashed-outlined insets, and full-

becoming activating its degradation in the absence of light. To assess this, we quantified cells under the same expression conditions but kept in the dark. Cells expressing TRIM21 in the dark presented a significantly lower percentage of adhered cells than non-expressing [–HS –MG +Light] cells (Figure 12B), suggesting that Ed-GFP basal degradation was indeed occurring. Nonetheless, light activation further disrupted Ed-mediated adhesions when compared to the dark condition, given that cells kept in the dark presented a significantly higher percentage of adhered cells (Figure 12B) and with generally stronger Ed-GFP expression relatively to light-activated induced [+HS –MG +Light] cells (Figure 12D & E).

Finally, we assessed whether proteasome inhibition by MG132 was able to rescue the adhesion phenotype. Surprisingly, proteasome inhibition in TRIM21 expressing cells [+HS +MG +Light] induced the lowest percentage of adhered cells out of all conditions (Figure 12B). When adhesions occurred, they were limited to very small portions of membrane (Figure 12F, arrows), and groups of more than two adhered cells were not present in the sample. This may be due to the presence of large aggregates of mRFP and GFP formed in the cells' cytoplasm (Figure 12F). Thus, aggregation in the absence of degradation was, in this context, an effective way of disrupting Ed-mediated adhesions. Importantly, proteasome-inhibited cells expressed much higher levels of V_HH mRFP-Cry2Clust-TRIM than the other co-transfected conditions. This could mean that basal degradation of V_HH mRFP-Cry2Clust-TRIM prior to light activation depleted the available pool of CRY2Clust-TRIM modules, thereby limiting the system's ability to correctly recruit Ed-GFP to the aggregates and therefore hindered overall efficiency.

CHAPTER V

Result discussion and future work

▪ Blank page ▪

Collectively, the results of this work show that it is possible to use a CRY2-based system to recruit proteins of interest tagged with GFP into light induced aggregates and subsequently target them for TRIM21-mediated proteasomal degradation.

TRIM21 C-terminal fusion to the light-induced homodimeriser CRY2Clust module is sufficient to elicit almost immediate clustering upon light exposure, and subsequent degradation of 70% of the initial pool of protein within 1 hour. The addition of further modules hindered overall degradation efficiency, highlighting the importance of the clustering process and the arrangement of the proteins within the light-induced clusters. Our initial results when comparing self-destabilisation of system components showed that the presence of more aggregate-inducing modules, such as CIBN-fused MP, did not result in a better degradation profile. One reason for this might be the fact that CIBN-MP produces large dodecameric oligomers (**S. Lee et al.**, 2014), which would then recruit the CRY2Clust-TRIM module, ultimately forming very large clusters loaded with a considerable amount of protein. Assuming that TRIM21 is recognising the whole aggregate for degradation, this may be overloading its activity by sheer protein excess, impairing overall efficacy. Another possibility is that TRIM21 inclusion in large aggregates might sterically hinder its accessibility by E2 ubiquitinases, delaying degradation.

Proteasome inhibition using MG132 confirmed that light-induced TRIM21-mediated degradation depends of the proteasomal system. Notably, TRIM21 has been reported to mediate not only proteasome targeting by Ub-^{48}Ub chains, but also the formation of so called non-canonical Ub-^{63}Ub chains (poly-Ub chains covalently linked by lysine 63) (**Fletcher et al.**, 2015), whose accumulation is particularly resistant to MG132 when compared to other Ub linkages, possibly resulting from an indirect response to proteasomal inhibition. This would also be consistent with TRIM21-mediated degradation being, in part, dependant on an alternative mechanism, such as the lysosomal pathway, in which the Ub^{63} linkage was shown to be involved (**Dammer et al.**, 2011). The involvement of alternative pathways of degradation should therefore not be excluded, and some substrates might be preferentially cleared through these non-canonical mechanisms. Whenever pertinent, putative involvement of the autophagy-lysosomal pathway can be tested using lysosome inhibitors, such as chloroquine or ammonium chloride (**Bonger et al.**, 2011).

We also attempted to determine the minimal functional unit of TRIM21 to induce degradation, and even though the CC and PRYSPRY domains proved to be unnecessary for the general use of our system, their removal lowered overall efficiency. This suggests that their presence could possibly introduce steric alterations or regulate interaction with other proteins, and thereby improve TRIM21 function in our application. Our results using the human sequence of the RING E3-ligase domain showed that, at least in *Drosophila* cells, human TRIM21 may be less prone to basal auto-degradation prior to light-induced clustering. Together with the fact that human TRIM21 is better described in terms of its domains and functionality of point mutants, which would facilitate fine tuning of the system's efficiency, these results might justify the use of human TRIM instead of mouse

TRIM21 in the future. Furthermore, because *Drosophila* cells do not express the protein, it would be interesting to compare RINGm against RINGh activity in mammalian systems, to check whether host cellular background has any effect on the application of light-induced degradation due to differential compatibility towards the introduced TRIM21 version.

Given that TRIM21 auto-ubiquitination occurs naturally in mammals with no compromise of its immune functions, the aspect of basal degradation raises a very relevant point for system design. Fletcher et al have proposed that the maintenance of auto-ubiquitinated TRIM21 levels is under tight regulation via synchronised sequential ubiquitination and deubiquitination (**Fletcher et al.**, 2015). The mechanisms by which endogenous TRIM21 targets its substrates to the proteasome but protects itself from degradation are not yet well understood (**Dickson et al.**, 2018), and its dual role as an anti-viral agent and transcription factor mediator complicates the dissection of TRIM's auto-ubiquitination roles (**Fletcher et al.**, 2015). Notably, it has been shown that Ab-bound viral capsids underwent rapid degradation, in the presence of TRIM21, but whereas both the Ab and the capsid were degraded, neither of them was ubiquitinated. This led the authors to suggest that TRIM21 might rely on auto-ubiquitination alone to target proteins for proteasomal degradation, unlike most E3 ubiquitin ligases, which transfer self-linked Ub chains onto their substrates (**Mallery et al.**, 2010). Surprisingly, endogenous and activated, auto-ubiquitinated TRIM21 displays very low turnover rates (**Dickson et al.**, 2018; **Mallery et al.**, 2010). Moreover, TRIM21 targeting of viral substrates for degradation does not require direct viral contact (**Mallery et al.**, 2010), leading some authors to suggest a "long-range" mechanism for TRIM21 target recognition and ubiquitination, in which stoichiometry and array disposition would play key roles (**Anandapadamanaban et al.**, 2019). In line with this possibility, our results showed that TRIM21 basal degradation does not compromise POI levels prior to system activation, and the constructs in which the degradation and the targeting modules were expressed separately were much less efficient at degradation than the tandem-fused V_HH-Cry2Clust-TRIM. In light of these results, we can speculate that aggregation acts as an onset trigger for substrate targeted degradation, and that the allosteric arrangement and/or the CRY2Clust:TRIM21 stoichiometry in the clusters affects TRIM21 activity towards the POI. On the other hand, high amount of non-clustered protein remained in the cytoplasm for these constructs, so we cannot rule out the possibility that impaired clustering and inefficient POI recruitment might also be the limiting step. Finally, the N-terminal fusion of other proteins to TRIM21 may be affecting its target recognition ability, E3 ligase activity and/or auto-ubiquitination when compared to endogenous TRIM21.

The multimeric nature of the light-induced clusters raises yet another relevant aspect, in light of our system's ability to elicit co-clustering of a POI together with its binding partners. For instance, we have shown that LARIAT-based clustering can recruit GFP-tagged aPKC together with Par6, and it is reasonable to assume that V_HH-CRY2Clust-TRIM would have the same capacity, possibly inducing the degradation of both proteins upon aggregation, similarly to what was reported for the AdPROM system (**Fulcher et al.**, 2016). V_HH-

CRY2Clust-TRIM might therefore act as a tool to target whole complexes for proteasomal degradation upon exposure to a light trigger.

Finally, we probed our system's ability to affect the function of a cell-cell adhesion molecule. Echinoid is part of a complex localised at adherens junctions (**Wei et al.**, 2005), and its involvement in intercellular adhesion poses a particularly challenging context for targeted depletion. For example, deGradFP, another V_HH-dependant system for targeted inducement of protein degradation, was unable to elicit depletion of a GFP-tagged version of another adherens junctions component, shotgun (*Drosophila* epithelial cadherin) (**Caussinus et al.**, 2012). The authors suggest that target proteins embedded in big protein complexes could place their GFP tag in such a position that hinders V_HH access. Our system was able to interfere with Ed-mediated adhesions in S2 cells and reduce the percentage of adhered cells by approximately 40%. However, basal TRIM21 activity was also able to interfere with cellular adhesion in the absence of light-induced system activation, albeit less effectively. One possibility is that V_HH recognition of GFP-tagged Ed in vesicles and cell-cell adhesions could generate a high local concentration of the V_HH-CRY2Clust-TRIM module, which would be sufficient to induce spontaneous, light-independent aggregation due to the homodimerisation capacity of CRY2 and TRIM21. Surprisingly, aggregation in the presence of MG132 proteasome inhibitor was more effective at disrupting Ed-mediated adhesions in this context. Proteasome-inhibited cells expressed much higher levels of V_HH mRFP-Cry2Clust-TRIM than the other conditions. Thus, it is likely that basal degradation of V_HH mRFP-Cry2Clust-TRIM prior to light activation depleted the available pool of CRY2Clust-TRIM modules, thereby limiting the system's ability to recruit Ed-GFP to the aggregates and therefore hindering overall efficiency degradation efficiency. Moreover, the formation of very large clusters in these cells highlighted the importance of coupling effective degradation to the clustering process, as these structures took up great portions of the cytoplasm, which would be incompatible, for example, with live imaging of many intracellular processes, not to mention the likely exertion of stress over cellular function and viability.

Overall, the fast kinetics of targeted degradation of GFP-tagged proteins of interest presented by the V_HH-CRY2CLust-TRIM21 system developed herein result in an unprecedented potential for acute disruption of protein function involved in highly dynamic processes. Complementation of these results from a biochemical point of view should follow to improve mechanistic understanding of the system, and facilitate future fine-tuning and optimisation.

▪ Blank page ▪

References

Akutsu, M., Dikic, I., & Bremm, A. (2016). Ubiquitin chain diversity at a glance. *Journal of Cell Science*, *129*(5), 875–880. https://doi.org/10.1242/jcs.183954

Anandapadamanaban, M., Kyriakidis, N. C., Csizmók, V., Wallenhammar, A., Espinosa, A. C., Ahlner, A., … Sunnerhagen, M. (2019). E3 ubiquitin-protein ligase TRIM21-mediated lysine capture by UBE2E1 reveals substrate-targeting mode of a ubiquitin-conjugating E2. *Journal of Biological Chemistry*, *294*(30), 11404–11419. https://doi.org/10.1074/jbc.RA119.008485

Banaszynski, L. A., & Wandless, T. J. (2006). Conditional Control of Protein Function. *Chemistry & Biology*, *13*(1), 11–21. https://doi.org/10.1016/j.chembiol.2005.10.010

Bence, M., Jankovics, F., Lukácsovich, T., & Erdélyi, M. (2017). Combining the auxin-inducible degradation system with CRISPR/Cas9-based genome editing for the conditional depletion of endogenous Drosophila melanogaster proteins. *The FEBS Journal*, *284*(7), 1056–1069. https://doi.org/10.1111/FEBS.14042@10.1111/(ISSN)1742-4658.EDITORSCHOICE2017

Bondeson, D. P., & Crews, C. M. (2017). Targeted Protein Degradation by Small Molecules. *Annual Review of Pharmacology and Toxicology*, *57*(1), 107–123. https://doi.org/10.1146/annurev-pharmtox-010715-103507

Bonger, K. M., Chen, L., Liu, C. W., & Wandless, T. J. (2011). Small-molecule displacement of a cryptic degron causes conditional protein degradation. *Nature Chemical Biology*, *7*(8), 531–537. https://doi.org/10.1038/nchembio.598

Campbell, A. E., & Bennett, D. (2016). Targeting protein function: the expanding toolkit for conditional disruption. *Biochemical Journal*, *473*(17), 2573–2589. https://doi.org/10.1042/BCJ20160240

Caussinus, E., Kanca, O., & Affolter, M. (2012). Fluorescent fusion protein knockout mediated by anti-GFP nanobody. *Nature Structural and Molecular Biology*, *19*(1), 117–122. https://doi.org/10.1038/nsmb.2180

Cesaratto, F., Burrone, O. R., & Petris, G. (2016). Tobacco Etch Virus protease: A shortcut across biotechnologies. *Journal of Biotechnology*, *231*, 239–249. https://doi.org/10.1016/j.jbiotec.2016.06.012

Clift, D., McEwan, W. A., Labzin, L. I., Konieczny, V., Mogessie, B., James, L. C., & Schuh, M. (2017). A Method for the Acute and Rapid Degradation of Endogenous Proteins. *Cell*, *172*(7), 1692-1706.e18. https://doi.org/10.1016/j.cell.2017.10.033

Dammer, E. B., Na, C. H., Xu, P., Seyfried, N. T., Duong, D. M., Cheng, D., … Peng, J. (2011). Polyubiquitin Linkage Profiles in Three Models of Proteolytic Stress Suggest the Etiology of Alzheimer Disease. *Journal of Biological Chemistry*, *286*(12), 10457–10465. https://doi.org/10.1074/jbc.M110.149633

Daniel, K., Icha, J., Horenburg, C., Müller, D., Norden, C., & Mansfeld, J. (2018). Conditional control of fluorescent protein degradation by an auxin-dependent nanobody. *Nature Communications*, *9*(1), 3297. https://doi.org/10.1038/s41467-018-05855-5

Dickson, C., Fletcher, A. J., Vaysburd, M., Yang, J. C., Mallery, D. L., Zeng, J., … James, L. C. (2018). Intracellular antibody signalling is regulated by phosphorylation of the Fc receptor TRIM21. *ELife*, *7*, 1–22. https://doi.org/10.7554/eLife.32660

Espinosa, A., Hennig, J., Ambrosi, A., Anandapadmanaban, M., Abelius, M. S., Sheng, Y., …

Wahren-Herlenius, M. (2011). Anti-Ro52 Autoantibodies from Patients with Sjögren's Syndrome Inhibit the Ro52 E3 Ligase Activity by Blocking the E3/E2 Interface. *Journal of Biological Chemistry*, *286*(42), 36478–36491. https://doi.org/10.1074/jbc.M111.241786

Espinosa, A., Zhou, W., Ek, M., Hedlund, M., Brauner, S., Popovic, K., … Wahren-Herlenius, M. (2006). The Sjögren's Syndrome-Associated Autoantigen Ro52 Is an E3 Ligase That Regulates Proliferation and Cell Death. *The Journal of Immunology*, *176*(10), 6277–6285. https://doi.org/10.4049/jimmunol.176.10.6277

Fisher, S. L., & Phillips, A. J. (2018). Targeted protein degradation and the enzymology of degraders. *Current Opinion in Chemical Biology*, *44*, 47–55. https://doi.org/10.1016/j.cbpa.2018.05.004

Fletcher, A. J., & James, L. C. (2016). Coordinated Neutralization and Immune Activation by the Cytosolic Antibody Receptor TRIM21. *Journal of Virology*, *90*(10), 4856–4859. https://doi.org/10.1128/JVI.00050-16

Fletcher, A. J., Mallery, D. L., Watkinson, R. E., Dickson, C. F., & James, L. C. (2015). Sequential ubiquitination and deubiquitination enzymes synchronize the dual sensor and effector functions of TRIM21. *Proceedings of the National Academy of Sciences*, *112*(32), 10014–10019. https://doi.org/10.1073/pnas.1507534112

Foss, S., Watkinson, R., Sandlie, I., James, L. C., Andersen, J. T., Watkinson, R., … Andersen, J. T. (2015). TRIM21: a cytosolic Fc receptor with broad antibody isotype specificity. *Immunological Reviews*, *268*(1), 328–339. https://doi.org/10.1111/imr.12363

Fulcher, L. J., Macartney, T., Bozatzi, P., Hornberger, A., Rojas-Fernandez, A., & Sapkota, G. P. (2016). An affinity-directed protein missile system for targeted proteolysis. *Open Biology*, *6*(10). https://doi.org/10.1098/rsob.160255

Gaj, T., Sirk, S. J., Shui, S.-L., & Liu, J. (2016). Genome-Editing Technologies: Principles and Applications. *Cold Spring Harbor Perspectives in Biology*, *8*(12). https://doi.org/10.1101/cshperspect.a023754

Harper, S. M. (2003). Structural Basis of a Phototropin Light Switch. *Science*, *301*(5639), 1541–1544. https://doi.org/10.1126/science.1086810

Heigwer, F., Port, F., & Boutros, M. (2018). RNA Interference (RNAi) Screening in Drosophila. *Genetics*, *208*(3), 853–874. https://doi.org/10.1534/genetics.117.300077

Hicke, L., & Dunn, R. (2003a). Regulation of Membrane Protein Transport by Ubiquitin and Ubiquitin-Binding Proteins. *Annual Review of Cell and Developmental Biology*, *19*(1), 141–172. https://doi.org/10.1146/annurev.cellbio.19.110701.154617

Hicke, L., & Dunn, R. (2003b). Regulation of Membrane Protein Transport by Ubiquitin and Ubiquitin-Binding Proteins. *Annual Review of Cell and Developmental Biology*, *19*(1), 141–172. https://doi.org/10.1146/annurev.cellbio.19.110701.154617

Hochstrasser, M. (1996). UBIQUITIN-DEPENDENT PROTEIN DEGRADATION. *Annual Review of Genetics*, *30*(1), 405–439. https://doi.org/10.1146/annurev.genet.30.1.405

Hörner, M., & Weber, W. (2012). Molecular switches in animal cells. *FEBS Letters*, *586*(15), 2084–2096. https://doi.org/10.1016/j.febslet.2012.02.032

James, L. C., Keeble, A. H., Khan, Z., Rhodes, D. A., & Trowsdale, J. (2007). Structural basis for PRYSPRY-mediated tripartite motif (TRIM) protein function. *Proceedings of the National Academy of Sciences*, *104*(15), 6200–6205. https://doi.org/10.1073/pnas.0609174104

Johnston, C. A., Hirono, K., Prehoda, K. E., & Doe, C. Q. (2009). Identification of an Aurora-

A/PinsLINKER/Dlg spindle orientation pathway using induced cell polarity in S2 cells. *Cell*, *138*(6), 1150–1163. https://doi.org/10.1016/j.cell.2009.07.041

Keeble, A. H., Khan, Z., Forster, A., & James, L. C. (2008). TRIM21 is an IgG receptor that is structurally, thermodynamically, and kinetically conserved. *Proceedings of the National Academy of Sciences of the United States of America*, *105*(16), 6045–6050. https://doi.org/10.1073/pnas.0800159105

Kennedy, M. J., Hughes, R. M., Peteya, L. A., Schwartz, J. W., Ehlers, M. D., & Tucker, C. L. (2010). Rapid blue-light–mediated induction of protein interactions in living cells. *Nature Methods*, *7*(12), 973–975. https://doi.org/10.1038/nmeth.1524

Klewer, L., & Wu, Y. (2019). Light-Induced Dimerization Approaches to Control Cellular Processes. *Chemistry – A European Journal*, *25*, chem.201900562. https://doi.org/10.1002/chem.201900562

Kolar, K., Knobloch, C., Stork, H., Žnidarič, M., & Weber, W. (2018). OptoBase: A Web Platform for Molecular Optogenetics. *ACS Synthetic Biology*, *7*(7), 1825–1828. https://doi.org/10.1021/acssynbio.8b00120

Lee, J., Natarajan, M., Nashine, V. C., Socolich, M., Vo, T., Russ, W. P., … Ranganathan, R. (2008). Surface sites for engineering allosteric control in proteins. *Science (New York, N.Y.)*, *322*(5900), 438–442. https://doi.org/10.1126/science.1159052

Lee, S., Park, H., Kyung, T., Kim, N. Y., Kim, S., Kim, J., & Heo, W. Do. (2014). Reversible protein inactivation by optogenetic trapping in cells. *Nature Methods*, *11*(6), 633–636. https://doi.org/10.1038/nmeth.2940

Mallery, D. L., McEwan, W. A., Bidgood, S. R., Towers, G. J., Johnson, C. M., & James, L. C. (2010). Antibodies mediate intracellular immunity through tripartite motif-containing 21 (TRIM21). *Proceedings of the National Academy of Sciences of the United States of America*, *107*(46), 19985–19990. https://doi.org/10.1073/pnas.1014074107

Maynard-Smith, L. A., Chen, L., Banaszynski, L. A., Ooi, A. G. L., & Wandless, T. J. (2007). A Directed Approach for Engineering Conditional Protein Stability Using Biologically Silent Small Molecules. *Journal of Biological Chemistry*, *282*(34), 24866–24872. https://doi.org/10.1074/jbc.M703902200

Natsume, T., & Kanemaki, M. T. (2017). Conditional Degrons for Controlling Protein Expression at the Protein Level. *Annual Review of Genetics*, *51*(1), 83–102. https://doi.org/10.1146/annurev-genet-120116-024656

Natsume, T., Kiyomitsu, T., Saga, Y., & Kanemaki, M. T. (2016). Rapid Protein Depletion in Human Cells by Auxin-Inducible Degron Tagging with Short Homology Donors. *Cell Reports*, *15*(1), 210–218. https://doi.org/10.1016/j.celrep.2016.03.001

Noda, Y., Kohjima, M., Izaki, T., Ota, K., Yoshinaga, S., Inagaki, F., … Sumimoto, H. (2003). Molecular recognition in dimerization between PB1 domains. *The Journal of Biological Chemistry*, *278*(44), 43516–43524. https://doi.org/10.1074/jbc.M306330200

Oke, V., & Wahren-Herlenius, M. (2012). The immunobiology of Ro52 (TRIM21) in autoimmunity: A critical review. *Journal of Autoimmunity*, *39*(1–2), 77–82. https://doi.org/10.1016/j.jaut.2012.01.014

Osswald, M., Santos, A. F., & Morais-de-Sá, E. (2019). Light-Induced Protein Clustering for Optogenetic Interference and Protein Interaction Analysis in Drosophila S2 Cells. *Biomolecules*, *9*(2), 61. https://doi.org/10.3390/biom9020061

Park, H., Kim, N. Y., Lee, S., Kim, N., Kim, J., & Heo, W. Do. (2017). Optogenetic protein

clustering through fluorescent protein tagging and extension of CRY2. *Nature Communications*, *8*(1), 30. https://doi.org/10.1038/s41467-017-00060-2

Pauli, A., Althoff, F., Oliveira, R. A., Heidmann, S., Schuldiner, O., Lehner, C. F., … Nasmyth, K. (2008). Cell-Type-Specific TEV Protease Cleavage Reveals Cohesin Functions in Drosophila Neurons. *Developmental Cell*, *14*(2), 239–251. https://doi.org/10.1016/j.devcel.2007.12.009

Piskadlo, E. (2017). *Maintenance of metaphase chromosome architecture by condensin I*. Universidade Nova de Lisboa.

Rakhit, R., Navarro, R., & Wandless, T. J. (2014). Chemical Biology Strategies for Posttranslational Control of Protein Function. *Chemistry & Biology*, *21*(9), 1238–1252. https://doi.org/10.1016/j.chembiol.2014.08.011

Rawlins, E. L., Lovegrove, B., & Jarman, A. P. (2003). Echinoid facilitates Notch pathway signalling during Drosophila neurogenesis through functional interaction with Delta. *Development (Cambridge, England)*, *130*(26), 6475–6484. https://doi.org/10.1242/dev.00882

Röth, S., Fulcher, L. J., & Sapkota, G. P. (2019). Advances in targeted degradation of endogenous proteins. *Cellular and Molecular Life Sciences*, *76*(14), 2761–2777. https://doi.org/10.1007/s00018-019-03112-6

Rothbauer, U., Zolghadr, K., Tillib, S., Nowak, D., Schermelleh, L., Gahl, A., … Leonhardt, H. (2006). Targeting and tracing antigens in live cells with fluorescent nanobodies. *Nature Methods*, *3*(11), 887–889. https://doi.org/10.1038/nmeth953

Rueden, C. T., Schindelin, J., Hiner, M. C., DeZonia, B. E., Walter, A. E., Arena, E. T., & Eliceiri, K. W. (2017). ImageJ2: ImageJ for the next generation of scientific image data. *BMC Bioinformatics*, *18*(1), 529. https://doi.org/10.1186/s12859-017-1934-z

Schindelin, J., Arganda-Carreras, I., Frise, E., Kaynig, V., Longair, M., Pietzsch, T., … Cardona, A. (2012). Fiji: an open-source platform for biological-image analysis. *Nature Methods*, *9*(7), 676–682. https://doi.org/10.1038/nmeth.2019

SerialBasics. (2012). Serial Cloner 2.6. Retrieved from http://serialbasics.free.fr/Serial_Cloner.html

Sigma-Aldrich. (2014). OligoEvaluator. Retrieved from https://www.sigmaaldrich.com/technical-documents/articles/biology/oligo-evaluator.html

Stothard, P. (2000). The Sequence Manipulation Suite: JavaScript Programs for Analyzing and Formatting Protein and DNA Sequences. *BioTechniques*, *28*(6), 1102–1104. https://doi.org/10.2144/00286ir01

Suzuki, A., Ishiyama, C., Hashiba, K., Shimizu, M., Ebnet, K., & Ohno, S. (2002). aPKC kinase activity is required for the asymmetric differentiation of the premature junctional complex during epithelial cell polarization. *Journal of Cell Science*, *115*(18), 3565–3573. https://doi.org/10.1242/jcs.00032

Toure, M., & Crews, C. M. (2016). Small-Molecule PROTACS: New Approaches to Protein Degradation. *Angewandte Chemie International Edition*, *55*(6), 1966–1973. https://doi.org/10.1002/anie.201507978

Wallenhammar, A., Anandapadamanaban, M., Lemak, A., Mirabello, C., Lundström, P., Wallner, B., & Sunnerhagen, M. (2017). Solution NMR structure of the TRIM21 B-box2 and identification of residues involved in its interaction with the RING domain. *PLOS*

ONE, *12*(7), e0181551. https://doi.org/10.1371/journal.pone.0181551

Wei, S.-Y., Escudero, L. M., Yu, F., Chang, L.-H., Chen, L.-Y., Ho, Y.-H., … Hsu, J.-C. (2005). Echinoid Is a Component of Adherens Junctions That Cooperates with DE-Cadherin to Mediate Cell Adhesion. *Developmental Cell*, *8*(4), 493–504. https://doi.org/10.1016/J.DEVCEL.2005.03.015

Xu, P., Duong, D. M., Seyfried, N. T., Cheng, D., Xie, Y., Robert, J., … Peng, J. (2009). Quantitative Proteomics Reveals the Function of Unconventional Ubiquitin Chains in Proteasomal Degradation. *Cell*, *137*(1), 133–145. https://doi.org/10.1016/j.cell.2009.01.041

▪ Blank page ▪

Supplementary Figures

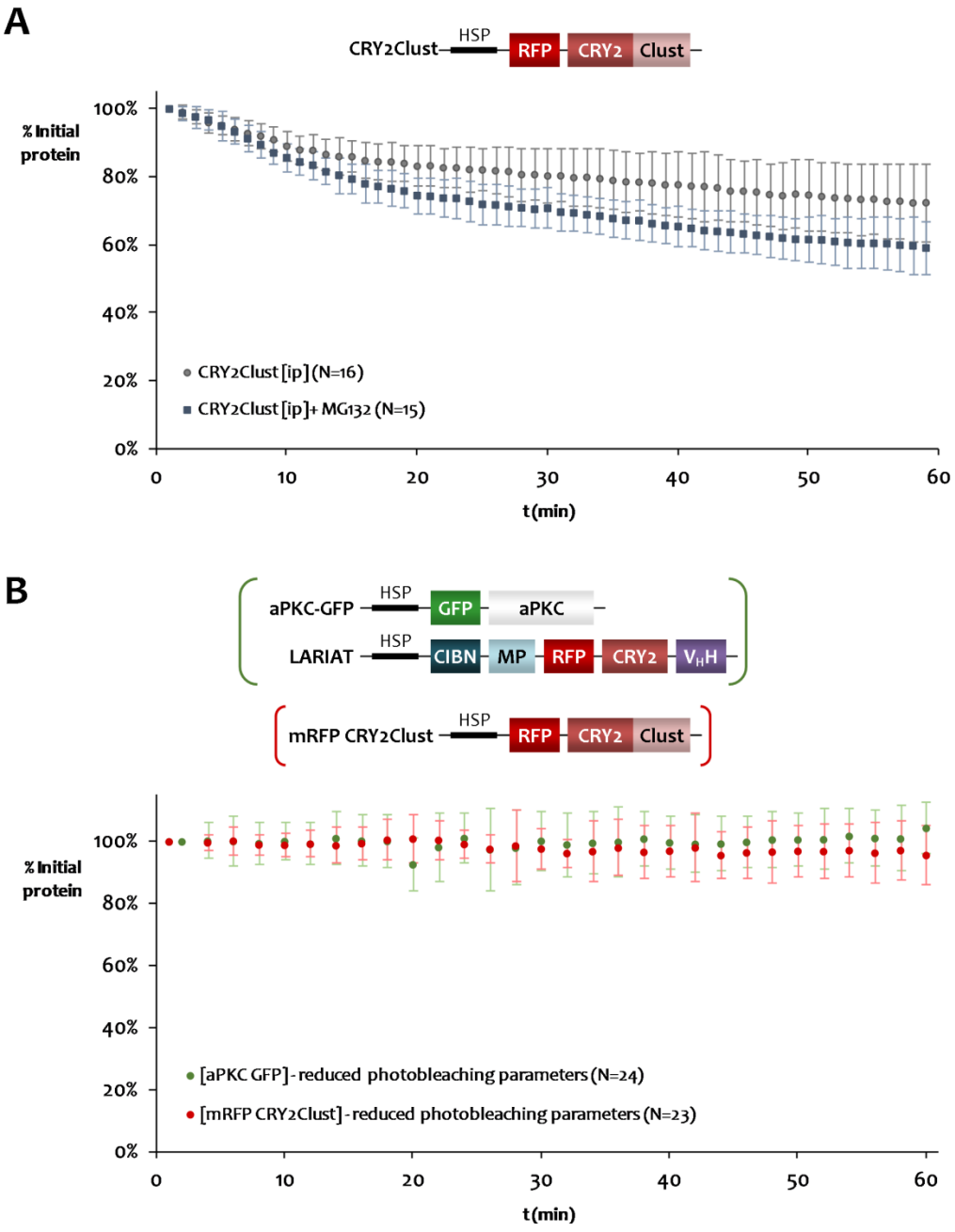

Supplementary Figure 1. Expression plots used for normalisation

(A) Intensity profiles used for normalisation of all timepoints acquired using initial acquisition parameters (ip): mRFP fluorescence intensity is plotted over time for the mRFP-CRY2Clust construct, with or without MG132.

(B) Intensity profiles used for normalisation of timepoints acquired using reduced photobleaching parameters (rp): mRFP fluorescence intensity plotted over time for the mRFP-CRY2Clust is shown in red and was used to normalise all mRFP intensities; GFP fluorescence intensity plotted over time for [GFP aPKC] (co-transfected with pLARIAT, to ensure aPKC clustering] is shown in green and was used to normalise all GFP intensities.

Supplementary movie legends

Movies S1 – S5. Live imaging of single S2 representative cells, related to Figure 5. mRFP expression of the indicated constructs is shown. Blue light (470nm) induced clustering was triggered at min 0. Initial parameters of acquisition were used. Scale bar = 2.5µm.

Movie S1. mRFP-CRY2Clust
Movie S2. mRFP-CRY2-TRIM
Movie S3. mRFP-CRY2Clust TRIM
Movie S4. CIBN-MP_ mRFP-CRY2Clust-TRIM
Movie S5. CIBN-TRIM_ mRFP-CRY2Clust

Movies S6 – S9. Live imaging of single S2 representative cells, related to Figure 6. mRFP expression of the indicated conditions is shown in (top) red, merged with green CellBrite membrane marker, and (bottom) greyscale. Blue light (470nm) induced clustering was triggered at min 0. Initial parameters of acquisition were used. Scale bar = 5µm.

Movie S6. mRFP-CRY2Clust
Movie S7. mRFP-CRY2Clust + MG132
Movie S8. mRFP-CRY2Clust TRIM
Movie S9. mRFP-CRY2Clust TRIM + MG132

Movies S10 & S11. Live imaging of single S2 representative cells, related to Figure 8. mRFP expression of the indicated constructs is shown. Blue light (470nm) induced clustering was triggered at min 0. Initial parameters of acquisition were used. Scale bar = 2.5µm.

Movie S10. mRFP-CRY2Clust-TRIM (ip)
Movie S11. mRFP-CRY2Clust-RING+BBox

Movies S12 - S14. Live imaging of single S2 representative cells, related to Figure 8. mRFP expression of the indicated constructs is shown. Blue light (470nm) induced clustering was triggered at min 0. Reduced photobleaching parameters of acquisition were used. Scale bar = 2.5µm.

Movie S12. mRFP-CRY2Clust-TRIM (rp)
Movie S13. mRFP-CRY2Clust-RINGm
Movie S14. mRFP-CRY2Clust-RINGh

Movies S15 & S16. Live imaging of single S2 representative cells, related to Figure 9. (**left**) GFP expression (**centre**) mRFP expression, and (**right**) merged GFP expression in green and mRFP expression in red are shown, for the indicated constructs, when co-transfected with LARIAT. Blue light (488nm) induced clustering was triggered at min 0. Scale bar = 2.5µm.

Movie S15. GFP-aPKC + Par6-mRFP
Movie S16. GFP-aPKCdN + Par6-mRFP

Movies S17 - S19. Live imaging of single S2 representative cells, related to Figure 10. (**left**) mRFP expression (**centre**) GFP expression, and (**right**) merged GFP expression in green and mRFP expression in red are shown, for the indicated constructs. Blue light (470nm) induced clustering was triggered at min 0. Reduced photobleaching parameters of acquisition were used. Scale bar = 2.5µm.

Movie S17. GFP-aPKC + VHH-mRFP-CRY2Clust-TRIM
Movie S18. GFP-aPKC + VHH-mRFP-CRY2Clust_CRY2Clust-TRIM
Movie S19. GFP-aPKC + mRFP-CRY2Clust-VHH_CRY2Clust-TRIM

Supplementary tables

Supplementary Table 1. Cell quantifications in Ed functional assay

		[–HS –MG +Light]	[+HS –MG +Light]	[+HS –MG –Light]	[+HS +MG +Light]
Number of total cells (T)		1 366	1 516	1 227	1 296
Number of GFP expressing cells (G)		260	-	-	-
Efficiency of GFP transfection (% G/T)			**19%**		
Efficiency of co-transfection (% GR/G)			**83%**		
Number of GFP&RFP positive cells (GR)	Measured	NA	-	-	205
	Theoretical (T x G/T x GR/G)	NA	240	194	-
Number of GFP expressing attached cells (A_G)		219	-	-	-
Attachment (% A_G/T)		**84%**	-	-	-
Number of GFP&RFP positive attached cells (A_{GR})		NA	107	115	33
Attachment (% A_{GR}/GR)		NA	**45%**	**59%**	**16%**